2022

Characterizing isoform switching events in esophageal adenocarcinoma

Yun Zhang

Katherine M. Weh

Connor L. Howard

Jean-Jack Riethoven

Jennifer L. Clarke

See next page for additional authors

Authors

Yun Zhang, Katherine M. Weh, Connor L. Howard, Jean-Jack Riethoven, Jennifer L. Clarke, Kiran H. Lagisetty, Jules Lin, Rishindra M. Reddy, Andrew C. Chang, David G. Beer, and Laura A. Kresty

Molecular Therapy
Nucleic Acids
Original Article

Characterizing isoform switching events in esophageal adenocarcinoma

Yun Zhang,[1,2] Katherine M. Weh,[1,2] Connor L. Howard,[1,2] Jean-Jack Riethoven,[3,4] Jennifer L. Clarke,[5] Kiran H. Lagisetty,[1,2] Jules Lin,[1,2] Rishindra M. Reddy,[1,2] Andrew C. Chang,[1,2] David G. Beer,[1,2] and Laura A. Kresty[1,2]

[1]Department of Surgery, Thoracic Surgery Section, University of Michigan, Ann Arbor, MI 48109, USA; [2]Rogel Cancer Center, University of Michigan, Ann Arbor, MI 48109, USA; [3]Nebraska Center for Biotechnology, University of Nebraska-Lincoln, Lincoln, NE 68588, USA; [4]Nebraska Center for Integrated Biomolecular Communication, University of Nebraska-Lincoln, Lincoln, NE 68588, USA; [5]Department of Food Science and Technology, University of Nebraska-Lincoln, Lincoln, NE 68588, USA

Isoform switching events with predicted functional consequences are common in many cancers, but characterization of switching events in esophageal adenocarcinoma (EAC) is lacking. Next-generation sequencing was used to detect levels of RNA transcripts and identify specific isoforms in treatment-naïve esophageal tissues ranging from premalignant Barrett's esophagus (BE), BE with low- or high-grade dysplasia (BE.LGD, BE.HGD), and EAC. Samples were stratified by histopathology and *TP53* mutation status, identifying significant isoform switching events with predicted functional consequences. Comparing BE.LGD with BE.HGD, a histopathology linked to cancer progression, isoform switching events were identified in 75 genes including *KRAS*, *RNF128,* and *WRAP53*. Stratification based on *TP53* status increased the number of significant isoform switches to 135, suggesting switching events affect cellular functions based on *TP53* mutation and tissue histopathology. Analysis of isoforms agnostic, exclusive, and shared with mutant *TP53* revealed unique signatures including demethylation, lipid and retinoic acid metabolism, and glucuronidation, respectively. Nearly half of isoform switching events were identified without significant gene-level expression changes. Importantly, two *TP53*-interacting isoforms, *RNF128* and *WRAP53*, were significantly linked to patient survival. Thus, analysis of isoform switching events may provide new insight for the identification of prognostic markers and inform new potential therapeutic targets for EAC.

INTRODUCTION

Esophageal cancer is the seventh most common cancer worldwide and one of the most lethal cancers.[1] The two main subtypes of esophageal cancer include adenocarcinoma (EAC) and squamous cell carcinoma (ESCC). Increasing incidence of EAC has been observed throughout Westernized countries, including the United States, United Kingdom, and Australia in recent years, whereas ESCC has been declining with reduced tobacco use.[2] EAC is the predominant subtype of esophageal cancer in the United States and the seventh leading cause of cancer-related deaths among US men.[3] Moreover, the 5-year survival rate following a diagnosis of EAC remains poor at 19.9%.[4] EAC is strongly associated with gastroesophageal reflux disease (GERD), obesity, and male gender, and frequently develops subsequent to long-standing Barrett's esophagus (BE).[5] BE is a metaplastic replacement of the normal squamous esophageal cells by specialized columnar epithelium, usually resulting from chronic GERD.[5,6] BE represents the only known precursor lesion to EAC.[7] Importantly, cancer risk and mutational burden increase with progression beyond BE metaplasia to BE with low-grade dysplasia (LGD) and high-grade dysplasia (HGD).[8,9] For BE patients with LGD, the incidence rate of EAC is as low as 1.70% per patient-year, whereas the incidence rate of EAC dramatically increases to 6.58% per patient-year among BE patients with HGD.[10] In addition, many patients diagnosed with BE and HGD have occult EAC, further supporting the elevated risk associated with BE accompanied by advanced pathologic changes.[11] For these reasons, increasing our understanding of the transition from low- to high-risk BE pathology or BE with LGD to HGD and EAC may identify patterns of progression and in turn facilitate early detection and potentially a window for intervention.

EAC is a cancer with one of the highest mutational burdens,[12,13] but unlike other similar cancers, the mutational burden is spread across a large number of genes with relatively low mutational frequencies, except for *TP53*.[13–16] This coupled with the high spatial and temporal heterogeneity of EAC has hampered clinical applications targeting mutational drivers.[17] Despite improved understanding of the genomic landscape contributing to progression from BE to EAC in recent years, we still have a poor understanding of how to leverage this information for improved risk stratification, or to inform targeted strategies for esophageal cancer prevention and treatment. Thus, in the current study we sought to move beyond single gene transcript analysis to characterize differential alternatively spliced isoforms of genes in esophageal tissues based on histological progression and *TP53* mutation status. This approach permits an investigation of

Received 9 February 2022; accepted 14 August 2022;
https://doi.org/10.1016/j.omtn.2022.08.018.

Correspondence: Laura A. Kresty, PhD, Department of Surgery, Thoracic Surgery Section, University of Michigan, Ann Arbor, MI 48109, USA.
E-mail: lkresty@med.umich.edu

A

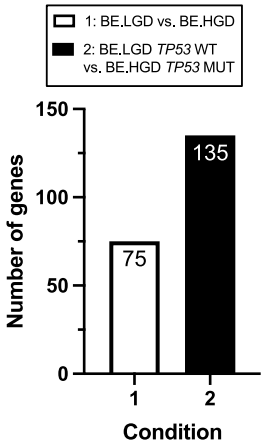

B

BE.LGD vs. BE. HGD GO PROCESSES (N = 75)	BE.LGD *TP53* WT vs. BE.HGD *TP53* MUT GO PROCESSES (N = 135)
Regulation of glucuronosyltransferase activity	Regulation of glucuronosyltransferase activity
Negative regulation of glucuronosyltransferase activity	Negative regulation of glucuronosyltransferase activity
Negative regulation of cellular glucuronidation	Negative regulation of cellular glucuronidation
Cellular glucuronidation	Cellular glucuronidation
Flavonoid glucuronidation	Retinoic acid metabolic process
Regulation of cellular glucuronidation	Regulation of cellular glucuronidation
Uronic acid metabolic process	Flavonoid glucuronidation
Glucuronate metabolic process	Uronic acid metabolic process
Xenobiotic glucuronidation	Glucuronate metabolic process
Flavonoid metabolic process	Xenobiotic glucuronidation

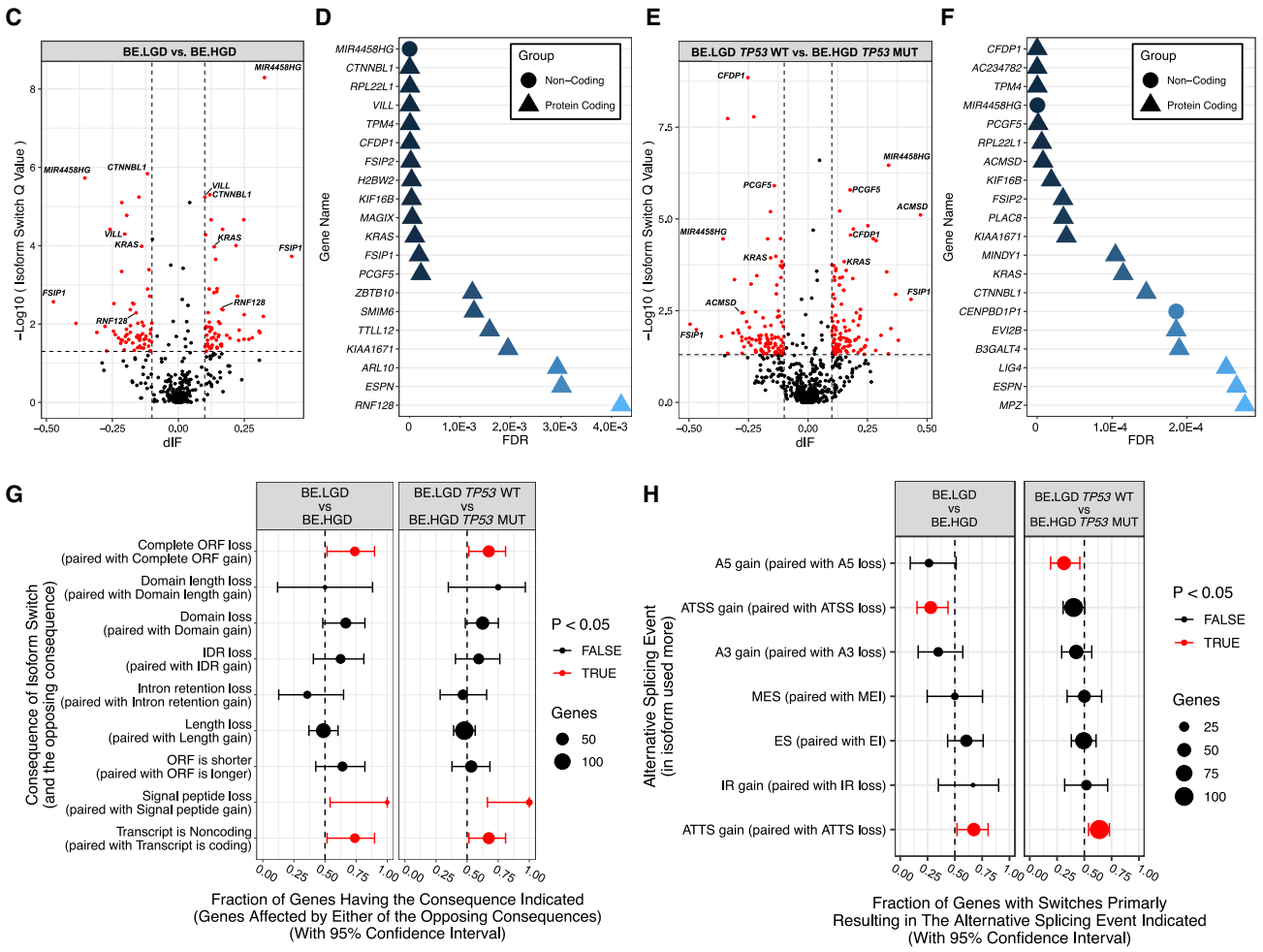

Figure 1. Identification of significant isoform switching events with predicted functional consequences based on histopathology and *TP53* status

(A) Number of isoform-switched genes detected in Barrett's esophagus with metaplasia and low-grade dysplasia (BE.LGD) compared with BE with high-grade dysplasia (BE.HGD) and with inclusion of *TP53* mutation status, wild-type (WT) or mutant (MUT). (B) Top 10 GO processes identified for each comparison ($p < 0.001$ and FDR <0.001), ranked by FDR value. (C) Volcano plot showing the differential isoform fraction (dIF) values comparing BE.LGD with BE.HGD. Each dot represents a transcript involved in isoform

(legend continued on next page)

the individual splice variants or isoforms that contribute to gene expression and in some cases reveals differentially expressed isoforms masked by unchanged gene expression.

Historically, the lack of functional annotation of gene isoforms and the dearth of sophisticated isoform analysis tools resulted in underutilization of RNA-sequencing (RNA-seq) data.[18] More recently, decreased sequencing costs coupled with increased availability of next-generation sequencing platforms and advanced RNA-seq analysis tools have made transcriptomics quantification with isoform resolution possible.[19] Several recent investigations have performed isoform switch analysis using TCGA data revealing that isoform switches are highly prominent in many cancers and can have profound biological impacts.[18,20,21] To date, comprehensive analysis of isoform switching has not been conducted in EAC or BE precursor lesions. Herein, we investigated isoform switching events using RNA-seq data collected from 57 esophageal tissue samples derived from 46 treatment-naïve patients undergoing esophagectomy following a diagnosis of HGD or EAC. Significant isoform switching events with predicted functional consequences were identified comparing patients stratified by histopathology and *TP53* mutation status. Multiple studies link aberrant *TP53* expression with malignant progression of BE, particularly BE with HGD.[22–26] Overall, *TP53* mutation remains the strongest known driver of EAC progression,[6] with a mutation frequency over 70% in EAC patients.[13] Incorporation of *TP53* mutation status in the analyses markedly increased detection of isoform-switched genes and expression of specific isoforms linked to *TP53* were significantly associated with patient survival. Gene Ontology (GO) enrichment analysis of genes associated with differential isoforms revealed both shared and unique cancer relevant alterations when comparing BE with LGD to BE with HGD histology. In turn, targeting identified processes may offer new leads for inhibiting BE progression. As proof-of-principle, we selected two novel agents informed by the study results and evaluated efficacy as inhibitors of EAC viability. Results indicate isoform switching events may provide new molecular insights and potentially identify prognostic markers or new therapeutic targets for EAC.

RESULTS

Isoform switching events and enrichment analysis based on histologic progression and *TP53*

Isoform switching analysis was performed comparing patient tissues categorized as BE with metaplasia and low-grade dysplasia (BE.LGD) to BE high-grade dysplasia (BE.HGD), alone or with stratification based on *TP53* mutation status as summarized in Figure 1. Patient demographic data and frequency of *TP53* mutation for each group are summarized in Table S1. When comparing BE.LGD with BE.HGD, 75 genes show significant isoform switching events with predicted functional consequences (Figure 1A). Moreover, with the inclusion of *TP53* mutation status, significant isoform switching events increased to 135 genes when comparing BE.LGD *TP53* wild-type (WT) with BE.HGD *TP53* mutant (MUT). Next, GO pathway enrichment analysis was performed (Figures 1B, Tables S2, and S3) revealing that most of the top enriched GO processes are shared between the two comparisons, with differences noted based on the significance of flavonoid metabolic process observed in BE.LGD versus BE.HGD and retinoic acid metabolic process observed in BE.LGD *TP53* WT versus BE.HGD *TP53* MUT. Dominant shared pathways included processes related to glucuronidation and metabolism. For BE.LGD versus BE.HGD, 14.7% (11 of 75) of top significant isoform-switched genes have an absolute differential isoform fraction (dIF) value greater than 0.25 (Figure 1C) and nearly all of the top 20 significant genes involved in isoform switching are protein-coding genes with the exception of *MIR4458HG* (Figure 1D). Similarly, when comparing BE.LGD *TP53* WT and BE.HGD *TP53* MUT, 17.0% (23 of 135) of top significant isoform-switched genes have an absolute dIF value greater than 0.25 (Figure 1E) and again protein-coding genes dominate, except for *MIR4458HG* and *CENPBD1P1* (Figure 1F). Among all identified isoform-switched genes, only isoform switching of *RNF128* was previously reported in HGD and EAC.[27] Despite well-characterized gene-level changes in *KRAS* with EAC progression, isoform switching events were not previously reported.[28–31] Additional isoform switch events reported previously in other cancer targets were also identified in our results, including *TPM4* and *MINDY1*.[27,32–36] Isoform switching of *TP53* is not observed in BE.LGD *TP53* WT versus BE.HGD *TP53* MUT, potentially because 84.6% (22/26) of *TP53* mutations are missense mutations failing to result in further transcriptional level changes in *TP53* isoforms (Figure S1). The high frequencies of missense *TP53* mutations and mutation hotspots observed in our cohort align with previously published studies in EAC.[37–39] Significant functional consequences associated with dominant isoforms identified in BE.HGD and BE.HGD *TP53* MUT include complete open reading frame (ORF) loss, signal peptide loss, and the loss of protein-coding isoforms (Figure 1G). Global splicing enrichment analysis also reveals that isoform switching events are significantly associated with changes in alternative transcription start sites (ATSS) and alternative transcription termination sites (ATTS) in BE.LGD versus BE.HGD, and changes in alternative 5′ splice site (A5) and ATTS in BE.LGD *TP53* WT versus BE.HGD *TP53* MUT (Figure 1H).

In addition, gene set enrichment analysis (GSEA) on RNA- and ribonucleoprotein (RNP)-related processes were performed on the gene-level data, as well as differential gene expression analysis on

switching. In red are isoforms with $|dIF| \geq 0.1$ and FDR ≤ 0.05. (D) Dot plot showing top 20 genes with significant isoform switching events for BE.LGD versus BE.HGD. The shape of each dot represents gene category and the color of each dot indicates significance level ($|dIF| \geq 0.1$ and FDR ≤ 0.05). (E) Volcano plot showing dIF values in BE.LGD *TP53* WT versus BE.HGD *TP53* MUT. Each dot represents a transcript involved in isoform switching. In red are isoforms with $|dIF| \geq 0.1$ and FDR ≤ 0.05. (F) Dot plot showing top 20 genes with significant isoform switching events BE.LGD *TP53* WT versus BE.HGD *TP53* MUT ($|dIF| \geq 0.1$ and FDR ≤ 0.05). (G) Dot plot showing functional consequences analysis associated with isoform switching. (H) Dot plot showing global alternative splicing event analysis. The size of the dot indicates the number of isoform-switched genes in each category and the line indicates 95% confidence interval. Significant changes in functional consequences and global alternative splicing events are colored in red ($p \leq 0.05$).

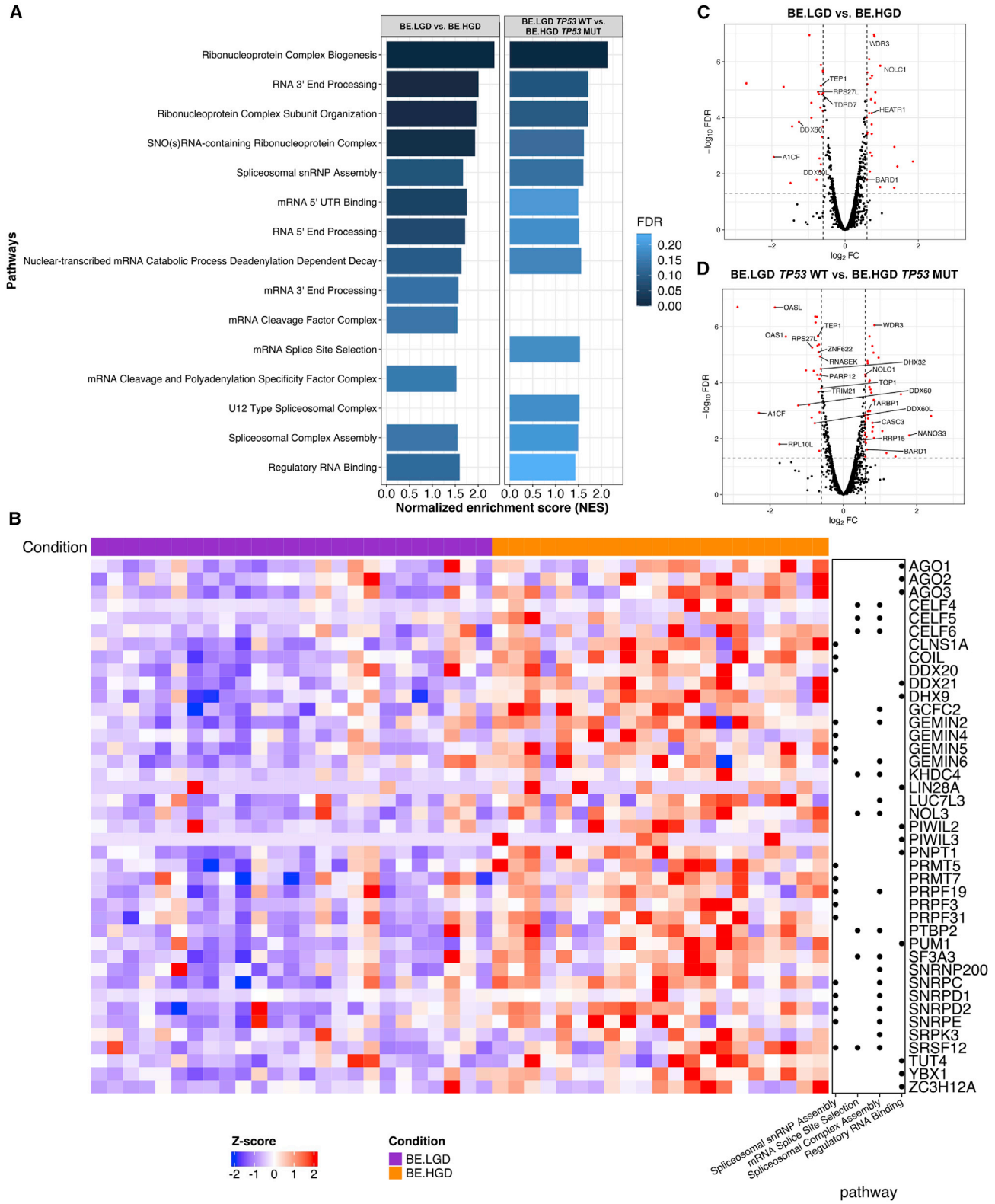

(legend on next page)

RNA-binding proteins (RBPs), because of the role that RNPs and RBPs play on alternative splicing.[40,41] GSEA analysis indicates significant enrichment of alternative-splicing-associated pathways, such as ribonucleoprotein complex biogenesis, spliceosomal small nuclear RNP (snRNP) assembly, mRNA splice site selection, and regulatory RNA binding (Figure 2A, Table S4, and S5). Sixty-one significant pathways were identified in BE.LGD versus BE.HGD, whereas 37 significant pathways were identified in BE.LGD *TP53* WT versus BE.HGD *TP53* MUT; thus, enriched pathways were more specific in BE.LGD *TP53* WT versus BE.HGD *TP53* MUT (Table S4 and S5). A strong upregulation of leading-edge genes in spliceosomal snRNP assembly, mRNA splice site selection, spliceosomal complex assembly, and regulatory RNA-binding pathways, as shown in Figures 2B is observed in BE.HGD compared with BE.LGD patient samples. Moreover, 54 and 73 RBPs are significantly differentially expressed in BE.LGD versus BE.HGD and BE.LGD *TP53* WT versus BE.HGD *TP53* MUT, respectively (Figures 2C and 2D). Among all identified RBPs, 18.5% (10 of 54) and 28.8% (21 of 73) of RBPs had predicted protein interactions with isoform-switched genes in BE.LGD versus BE.HGD and BE.LGD *TP53* WT versus BE.HGD *TP53* MUT, respectively. Taken together, both GSEA and differential gene expression analysis revealed that expression changes of RNA regulatory proteins and RBPs may contribute to observed isoform switching events.

Last, qRT-PCR was used to validate isoform switching of *RNF128*, *KRAS*, and *TRIM29* using a subset of patients in the cohort (Figure S2). Isoform fractions using qRT-PCR results were comparable to isoform fractions using RNA-seq data by the analysis tool.

Significant isoform switching events without differential gene expression

Interestingly, 42.7% (32 of 75) of significant isoform-switched genes in BE.LGD versus BE.HGD (Table 1) and 45.9% (62 of 135) of genes in BE.LGD *TP53* WT versus BE.HGD *TP53* MUT (Table 2) are not differentially expressed on the gene level between the two conditions. GO enrichment analysis was performed for isoform-switched genes that occur in the absence of gene-level expression changes (Tables 1 and 2), with results closely paralleling those shown in Figure 1B (data not shown). In brief, isoform switch analysis independent of gene-level changes in BE.LGD versus BE.HGD supported top enriched biologic processes focused on hormone-related processes, cellular glucuronidation, and histone and protein demethylation and dealkylation processes. Similarly, isoform-switched genes identified in the comparison of BE.LGD *TP53* WT versus BE.HGD *TP53* MUT without gene-level alterations show GO biologic processes overlapping with those in Figure 1B, but with less statistical significance likely due to reduced power with decreased sample numbers (data not shown).

Moreover, several identified isoform-switched genes that do not show overall differential gene expression have documented interactions with *TP53*, including *WRAP53*, *KDM6B,* and *TRIM29* (Figures 1D and 1F, Tables 1 and 2, and Figure S3). These data highlight the potential impact of stratifying the isoform data by *TP53* mutational status, as multiple isoform changes in *TP53*-related genes were identified that otherwise would go undetected.

Isoform switching events unique or shared based on stratification by pathology and *TP53* status

Although a large overlap was observed in GO enrichment analysis in BE.LGD versus BE.HGD (n = 75) compared with BE.LGD *TP53* WT versus BE.HGD *TP53* MUT (n = 135), the number of isoform switching events nearly doubled when *TP53* stratification was incorporated. Thus, a Venn diagram was generated to identify shared and unique isoform-switched genes in the analysis as shown in Figure 3A. Among all significant genes in the analysis, 60 isoform-switched genes are shared between the two comparisons (Figures 3A and Table S6), with 15 unique genes identified in BE.LGD versus BE.HGD (Figures 3A and Table S7), and 75 genes uniquely identified in BE.LGD *TP53* WT versus BE.HGD *TP53* MUT (Figures 3A and Table S8). As shown in Figure 3A, 80% (60 of 75) of the isoform-switched genes in BE.LGD versus BE.HGD are shared, whereas only 44.4% (60 of 135) of the isoform-switched genes in BE.LGD *TP53* WT versus BE.HGD *TP53* MUT are shared, supporting that greater numbers of unique alterations are associated with mutant *TP53*. Top significant genes in each section of the Venn diagram include many protein-coding genes, but also several non-protein-coding genes including *SNHG18*, *AC009509, CADM3-AS1, MIR4458HG, CENPBD1P1*, and *LINC02615* (Figures 3B–3D). Previously reported genes involved in isoform switching (*RNF128*, *TPM4*, and *KRAS*) were shared between the two comparisons, with the exception of *MINDY1,* which was uniquely identified in BE.LGD *TP53* WT versus BE.HGD *TP53* MUT.[27,32–36] Next, GO enrichment analysis of the non-overlapping isoforms in BE.LGD versus BE.HGD and BE.LGD *TP53* WT versus BE.HGD *TP53* MUT comparisons were conducted. For genes uniquely identified in BE.LGD versus BE.HGD, top enriched processes are related to histone and protein demethylation, dealkylation, and GDP catabolic process (Figure 3E and Table S9). Top enriched processes based on genes unique in BE.LGD *TP53* WT versus BE.HGD *TP53* MUT are more strongly associated with lipid and alcohol metabolism, retinoic acid metabolism and biosynthesis, and midgut development (Figure 3E).

Figure 2. Changes associated with RNA regulatory proteins and RNA-binding proteins on the gene-level data

(A) GO pathway enrichments associated with RNA regulatory proteins identified in BE.LGD versus BE.HGD and BE.LGD *TP53* WT versus BE.HGD *TP53* MUT (p-value $\leq$ 0.05 and FDR $\leq$0.25). Pathways are colored and ranked by FDR. (B) Heatmap of the leading-edge genes identified in select pathways in the GO pathway enrichment analysis. Dot plot on the right shows the pathways that the gene belongs. (C) Volcano plot of the expression of RNA-binding proteins (RBPs) in BE.LGD versus BE.HGD. (D) Volcano plot of the expression of RBPs in BE.LGD *TP53* WT versus BE.HGD *TP53* MUT. Red dot represents significantly differentially expressed RBPs ($|\log_2 FC| > 0.585$ and FDR $\leq$0.05). Gene names of the genes that interact with isoform-switched genes predicted by the STRING database are shown.

Table 1. Significant isoform switching events without altered gene expression in BE.LGD versus BE.HGD

Gene name	Isoform ID	dIF	FDR	Gene name	Isoform ID	dIF	FDR
MIR4458HG	ENST00000502001	0.326	<0.001	*KDM6B*	ENST00000254846	−0.123	0.020
	ENST00000652260	−0.355	<0.001		ENST00000575521	0.146	0.039
RPL22L1	ENST00000463836	−0.149	<0.001	*AC103810.1*	ENST00000585187	−0.201	0.021
	ENST00000475836	0.124	<0.001	*PCSK5*	ENST00000376752	0.134	0.022
AC234782.4	ENST00000674488	−0.259	<0.001		ENST00000674117	−0.147	0.023
	ENST00000674271	0.248	0.024	*AC073896.1*	ENST00000548360	0.125	0.023
SLC25A35	ENST00000581320	0.152	0.009		ENST00000549318	−0.124	0.024
	ENST00000577745	−0.131	0.025	*HSD11B1*	ENST00000615289	0.195	0.023
ZNF350	ENST00000243644	−0.138	0.009		ENST00000367027	−0.199	0.029
	ENST00000599258	0.125	0.013	*RBP2*	ENST00000511956	0.267	0.024
SNHG18	ENST00000508179	0.157	0.010	*AC009509.2*	ENST00000536922	0.229	0.026
	ENST00000655411	−0.246	0.015	*UGT2B7*	ENST00000305231	−0.217	0.026
TMEM104	ENST00000335464	−0.182	0.011	*GHR*	ENST00000537449	−0.147	0.026
	ENST00000584246	0.119	0.016	*SLC2A5*	ENST00000484798	−0.219	0.031
COX19	ENST00000466146	0.117	0.012	*AP000866.2*	ENST00000504932	0.163	0.033
WRAP53	ENST00000316024	0.126	0.014	*CADM3-AS1*	ENST00000415675	−0.128	0.033
	ENST00000396463	−0.154	0.040		ENST00000609696	0.128	0.035
DISP2	ENST00000559721	0.230	0.014	*RSPH1*	ENST00000291536	0.101	0.038
LINC02542	ENST00000660534	−0.195	0.019	*CFAP46*	ENST00000486104	−0.132	0.041
	ENST00000668266	0.120	0.042	*CA4*	ENST00000585705	0.147	0.041
NEU4	ENST00000407683	−0.239	0.019	*CNTN1*	ENST00000347616	−0.167	0.047
AC093866.1	ENST00000513572	0.153	0.019	*RTN2*	ENST00000245923	−0.105	0.048
	ENST00000612706	−0.102	0.028	*NUDT18*	ENST00000613958	0.108	0.049
GDF15	ENST00000252809	−0.145	0.020		ENST00000611621	−0.108	0.049

For genes shared between the two comparisons in the overlapping section of the Venn diagram, GO enriched processes are similar to the previous analysis (Figure 1B) with top processes related to glucuronidation and metabolism (Figures 3E and Table S10). Although enriched processes had a significant p-value (≤ 0.05), none of the enriched processes unique to BE.LGD *TP53* WT versus BE.HGD *TP53* MUT reached a significant false discovery rate (FDR) ≤ 0.05, but instead ranged from 0.08 to 0.16, suggesting greater heterogeneity of isoform-enriched genes in that grouping.

TP53-linked isoform changes correspond to patient outcomes

TP53 is the strongest known genetic driver of EAC with a mutation frequency of over 70% in EAC patients.[8,13] In turn, isoform-switched genes with direct interaction with *TP53* were identified using the STRING database (Figure S3). Patient survival was also determined to investigate whether there is an association between expression of specific isoforms of *TP53*-linked genes and survival among EAC patients.

Isoform switching of *RNF128* was recently reported to show decreased expression of *RNF128-202* and increased expression of *RNF128-201* contributing to the stabilization of mutant *TP53* and potentially EAC progression.[27] Our analysis confirms the *RNF128* isoform-switching event with similar trends observed (Figure 4A). The overall expression of *RNF128* is significantly lower in patients with BE.HGD compared with patients with BE.LGD and isoform usage of each isoform is significantly altered, supporting the isoform switching event. Functional domain prediction using Pfam did not reveal any major changes in protein domains. However, a significant difference in patient survival was observed in the analysis (Figure 4B). Patients with higher expression levels of *RNF128-202* had a significantly higher survival probability compared with patients with lower expression of the same isoform (Wilcoxon p-value = 0.031). Patient samples with high expression of *RNF128-202* were largely composed of BE.LGD samples with only one BE.HGD and one EAC patient sample, whereas tissues with low expression levels of *RNF128-202* were contributed by either BE.HGD or EAC samples.

WRAP53 is another isoform-switched gene with direct *TP53* interactions (Figure S3). *WRAP53* transcripts with exon regions overlapping with the *TP53* exon are believed to be the antisense of *TP53*, which can result in *TP53* induction.[42] On the gene level, significant expression differences were not observed in *WRAP53* between BE.LGD and BE.HGD patient samples. However, on the isoform level,

Table 2. Significant isoform switching without altered gene expression in BE.LGD *TP53* WT versus BE.HGD *TP53* MUT

Gene name	Isoform ID	dIF	FDR	Gene name	Isoform ID	dIF	FDR
MIR4458HG[a]	ENST00000502001	0.326	<0.001	*NEU4*[a]	ENST00000407683	−0.239	0.019
	ENST00000652260	−0.355	<0.001	*FSIP2-AS1*	ENST00000429929	−0.152	0.019
MINDY1	ENST00000361936	−0.135	<0.001	*AC015802.4*	ENST00000592622	−0.200	0.019
	ENST00000470877	0.100	<0.001	*ALDH1A2*	ENST00000558239	0.110	0.019
EVI2B	ENST00000330927	0.108	<0.001	*PTRH1*	ENST00000543175	0.202	0.019
	ENST00000577894	−0.108	<0.001	*ZNF324*	ENST00000196482	0.136	0.020
CENPBD1P1	ENST00000493504	−0.103	<0.001		ENST00000593925	−0.126	0.034
	ENST00000651608	0.117	<0.001	*GDF15*[a]	ENST00000252809	−0.145	0.020
AC234782.4[a]	ENST00000674488	−0.259	<0.001	*AC103810.1*[a]	ENST00000585187	−0.201	0.021
	ENST00000674271	0.248	0.024	*PCSK5*[a]	ENST00000376752	0.134	0.022
LINC02615	ENST00000505133	0.110	<0.001		ENST00000674117	−0.147	0.023
	ENST00000513851	−0.157	0.024	*DCDC2*	ENST00000378454	0.174	0.022
TSPAN6	ENST00000494424	−0.114	<0.001		ENST00000378450	−0.177	0.025
	ENST00000614008	0.108	0.021	*LTB4R2*	ENST00000527924	0.108	0.023
SMIM6	ENST00000556126	0.116	0.001	*CRYBA2*	ENST00000392096	−0.202	0.024
	ENST00000579469	−0.116	0.001	*GHR*[a]	ENST00000537449	−0.147	0.026
SESN1	ENST00000436639	−0.133	0.001	*NEURL2*	ENST00000545238	−0.240	0.028
TMED1	ENST00000588289	0.103	0.002		ENST00000372518	0.240	0.029
	ENST00000214869	−0.113	0.019	*MSH5-SAPCD1*	ENST00000476085	−0.137	0.028
AC026254.2	ENST00000666005	0.220	0.003		ENST00000493662	0.106	0.031
LINC00964	ENST00000657752	−0.128	0.005	*TNNI1*	ENST00000622580	−0.180	0.029
	ENST00000663940	0.107	0.009		ENST00000555340	0.164	0.043
TMEM241	ENST00000577448	0.100	0.005	*SFTA2*	ENST00000634371	−0.113	0.030
	ENST00000475185	0.128	0.029		ENST00000359086	0.106	0.037
PLA2G15	ENST00000562966	0.103	0.006	*CCDC170*	ENST00000537358	−0.269	0.030
	ENST00000219345	−0.115	0.044	*TLCD1*	ENST00000292090	0.153	0.031
ANKRD54	ENST00000609706	0.125	0.006	*SOCS4*	ENST00000395472	0.121	0.031
ZNF350[a]	ENST00000243644	−0.138	0.009	*AP000866.2*[a]	ENST00000504932	0.163	0.033
	ENST00000599258	0.125	0.013	*C1orf53*	ENST00000436652	0.147	0.033
GAS2	ENST00000278187	0.155	0.009	*TRIM29*	ENST00000532195	−0.122	0.036
ATP9B	ENST00000586722	0.115	0.009	*EFHC2*	ENST00000420999	0.221	0.037
SPATA17	ENST00000470448	0.118	0.011		ENST00000343571	−0.221	0.038
	ENST00000491809	−0.186	0.048	*RSPH1*[a]	ENST00000291536	0.101	0.038
TMEM104[a]	ENST00000335464	−0.182	0.011	*CARNS1*	ENST00000307823	−0.190	0.040
	ENST00000584246	0.119	0.016	*CFAP46*[a]	ENST00000486104	−0.132	0.041
COX19[a]	ENST00000466146	0.117	0.012	*CA4*[a]	ENST00000585705	0.147	0.041
WRAP53[a]	ENST00000316024	0.126	0.014	*ONECUT1*	ENST00000305901	−0.219	0.043
	ENST00000396463	−0.154	0.040	*LINC00278*	ENST00000652068	−0.135	0.043
DISP2[a]	ENST00000559721	0.230	0.014	*TMEM107*	ENST00000437139	0.106	0.045
BCL7A	ENST00000432926	−0.197	0.015	*ZBTB18*	ENST00000622512	−0.102	0.046
	ENST00000261822	0.160	0.039		ENST00000358704	0.102	0.047
AC117453.1	ENST00000651749	−0.182	0.016	*RTN2*[a]	ENST00000245923	−0.105	0.048
	ENST00000656199	0.151	0.021	*LINC01186*	ENST00000670979	0.115	0.049

(*Continued on next page*)

Table 2. *Continued*

Gene name	Isoform ID	dIF	FDR	Gene name	Isoform ID	dIF	FDR
SYT15	ENST00000449358	−0.138	0.017	*CCDC190*	ENST00000524710	−0.139	0.050
	ENST00000374321	0.131	0.026				
S100A5	ENST00000368717	−0.247	0.017				
	ENST00000368718	0.247	0.020				

[a]Genes shared between BE.LGD versus BE.HGD and BE.LGD *TP53* WT versus BE.HGD *TP53* MUT. BE.LGD: Barrett's esophagus with metaplasia or low-grade dysplasia; BE.HGD: Barrett's esophagus with high-grade dysplasia.

a significant increase of *WRAP53-201* and a decrease of *WRAP53-202* are observed (Figure 4C). The 5′-UTR of *WRAP53-201* contains a shared region with the first exon of *TP53*, whereas *WRAP53-202* does not have any overlapping regions. Moreover, patients with high expression levels of *WRAP53-201* have a significantly lower survival probability compared with patients with low expression levels of *WRAP53-201* (Figure 4D; Wilcoxon p-value = 0.050). All high-expressing patient samples were either BE.HGD or EAC, whereas low-expressing samples were contributed by BE.LGD tissues. Still, two BE.HGD patient samples and one EAC sample had low *WRAP53-201* expressions, suggesting isoform expression level is not solely determined by histopathological progression.

In addition, survival differences based on histopathological categorization were calculated to evaluate the possibility that significant differences in patient survival were solely driven by the histopathological distribution. The survival probability of patients with BE.HGD is marginally lower than the survival probability of BE.LGD patients (Figure 4E; Wilcoxon p-value = 0.113) and when EAC samples are included in the analysis, the survival probability is also marginally lower and borderline statistically significant (Figure 4F; Wilcoxon p-value = 0.058). Ultimately, these results support that isoform switching events may reveal specific gene isoforms that impact patient survival to a greater extent than histopathological changes alone and specific isoforms may be targetable as novel targets for prevention or treatment.

Isoform switching informs targetable processes for EAC inhibition

Our results revealed that mutant *TP53* increases isoform switching events and modulates numerous lipid and retinoic acid-linked processes including unique changes in 9-cis-retinoic acid, leading us to evaluate the inhibitory potential of two Food and Drug Administration (FDA)-approved and mechanistically relevant pharmacological agents for targeting EAC. *TP53* MUT EAC cells (OE33 and JHAD1) were treated with adapalene,[43] an agonist of the retinoic acid receptor (RAR) β and γ, and the mutant *TP53* targeting agent APR-246.[44] These two drugs were selected as proof-of-concept agents given identification of 9-cis-retinoic acid metabolic processes and retinoic acid biosynthetic processes in the comparison of BE.LGD *TP53* WT versus BE.HGD *TP53* MUT (Figure 3E). Gene-level GSEA reveals significant downregulation of retinol metabolism in BE.HGD *TP53* MUT patients compared with BE.LGD *TP53* WT (Figure S4), suggesting that activation of retinoic acid signaling may elicit anti-cancer activity targeting EAC. Therefore, adapalene was used to test whether stimulating retinoic acid signaling in *TP53* MUT EAC cell lines would induce EAC cell death. Both OE33 and JHAD1 cells show dose-dependent inhibition of viability following adapalene treatment with the lethal dose 50 (LD_{50}) in the 1.5- to 2.0-μM range (Figures 5A–5D). At 72 h post-treatment, 1.5 μM adapalene significantly decreases OE33 cell viability to 42.59% (Figures 5A and 5B). Similarly, at 72 h, 2.0 μM adapalene treatment significantly decreases JHAD1 cell viability to 41.50% (Figures 5C and 5D). Importantly, OE33 cells treated with adapalene do not recover following treatment removal (Figures S5A and S5B). However, JHAD1 cells do show recovery upon adapalene removal, suggesting adapalene is only inhibitory in JHAD1 cells when present, with little durable effect once removed (Figures S5C and S5D). Thus, a combination of agents may prove more efficacious in JHAD1 cells.

Next, APR-246, a small molecule agent that restores *TP53* WT functions in *TP53* MUT cells by covalently binding to cysteine residues in *TP53* MUT cells,[44] was evaluated. *TP53* mutation is a well-known driver for EAC progression and several isoform-switched genes have direct interactions with *TP53* (Figure S3). OE33 and JHAD1 cells were treated with various concentrations of APR-246. APR-246 treated OE33 cells show a dose-dependent response with an LD_{50} above 20 μM, but clearly less than 40 μM, which permanently induces cell death (Figures 5E, 5F, S5E, and S5F). At 72 h, 20 μM APR-246 treatment significantly decreased OE33 cell viability to 62.84% and 40 μM APR-246 treatment significantly decreased OE33 cells viability to 8.57%. OE33 cells treated with 40 μM APR-246 do not recover upon treatment withdrawal (Figures S5E and S5F). For JHAD1 cells, a sharp decrease in cell viability was observed between 20 μM and 40 μM treatments. At 72 h, 20 μM APR-246 treatment significantly decreases cell viability to 64.61%, whereas 40 μM treatment completely eradicates JHAD1 cells (Figures 5G and 5H). JHAD1 cells did recover following drug removal when lower concentrations of APR-246 were utilized (<40 μM; Figures S5G and S5H). Representative fluorescent images from the viability assays performed in OE33 and JHAD1 cells show decreases in viability from adapalene (Figures 5B and 5D) and APR-246 (Figures 5F and 5H). Collectively, these results confirm that targeting the retinoic acid and *TP53* pathways using pharmacological agents is successful in inducing EAC cancer cell death, and that evaluations

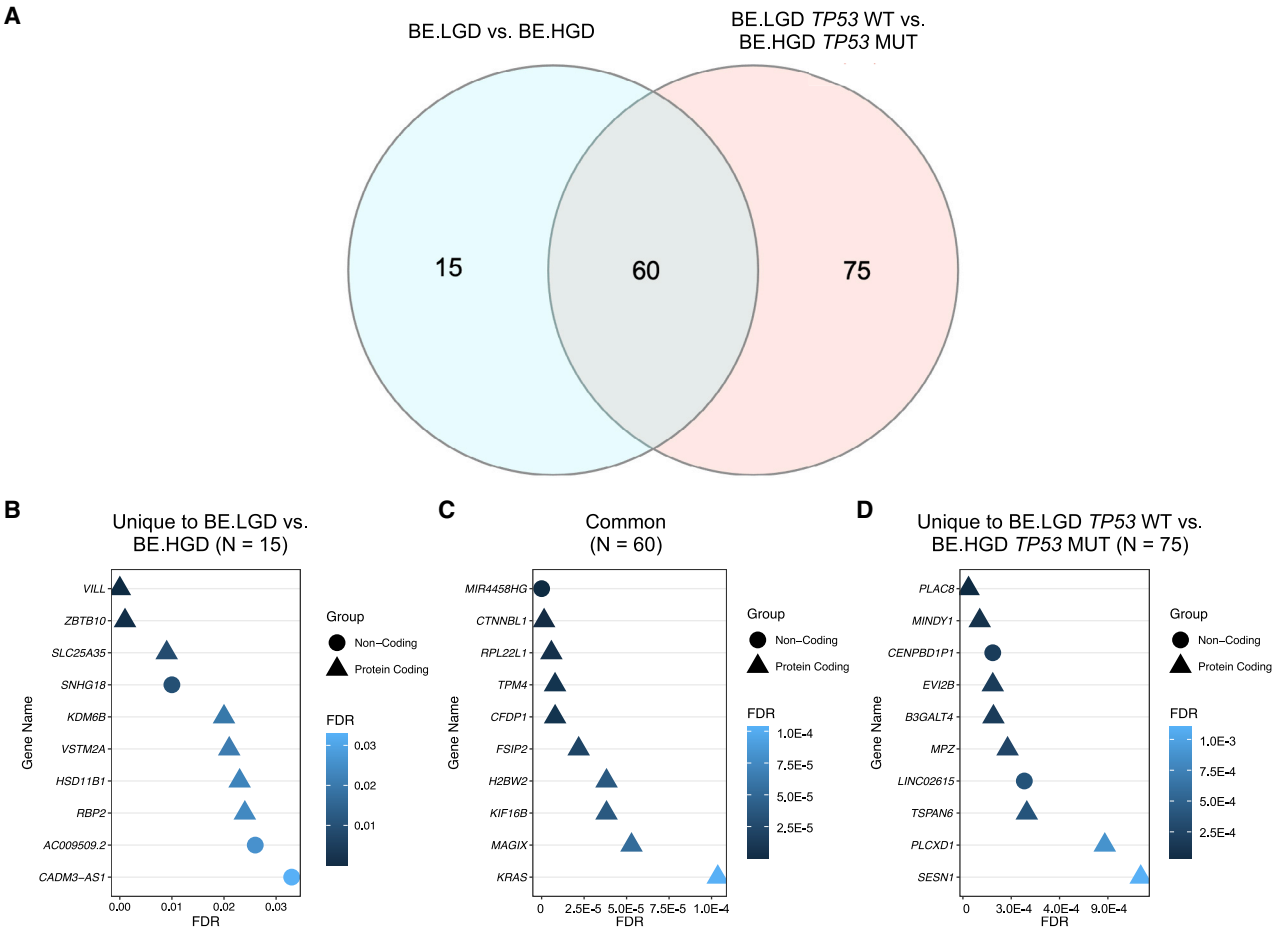

E

UNIQUE TO BE.LGD VS. BE.HGD	*P*-VALUE	FDR	COMMON	*P*-VALUE	FDR	UNIQUE TO BE.LGD *TP53* WT VS. BE.HGD *TP53* MUT	*P*-VALUE	FDR
Histone lysine demethylation	<0.01	0.02	Cellular glucuronidation	<0.01	<0.01	Lipid metabolic process	<0.01	0.08
Histone demethylation	<0.01	0.02	Regulation of glucuronosyltransferase activity	<0.01	<0.01	9-cis-retinoic acid metabolic process	<0.01	0.08
Protein demethylation	<0.01	0.02	Negative regulation of glucuronosyltransferase activity	<0.01	<0.01	cGMP catabolic process	<0.01	0.08
Protein dealkylation	<0.01	0.02	Negative regulation of cellular glucuronidation	<0.01	<0.01	9-cis-retinoic acid biosynthetic process	<0.01	0.08
Deoxyribonucleoside diphosphate catabolic process	<0.01	0.03	Uronic acid metabolic process	<0.01	<0.01	Midgut development	<0.01	0.08
dADP catabolic process	<0.01	0.03	Glucuronate metabolic process	<0.01	<0.01	Primary alcohol metabolic process	<0.01	0.09
Purine deoxyribonucleoside diphosphate catabolic process	<0.01	0.03	Flavonoid glucuronidation	<0.01	<0.01	Retinoic acid biosynthetic process	<0.01	0.12
dGDP catabolic process	<0.01	0.03	Regulation of cellular glucuronidation	<0.01	<0.01	Diterpenoid biosynthetic process	<0.01	0.12
GDP catabolic process	<0.01	0.03	Xenobiotic glucuronidation	<0.01	<0.01	Retinol metabolic process	<0.01	0.14
Demethylation	<0.01	0.03	Flavonoid metabolic process	<0.01	<0.01	Phagosome maturation	<0.01	0.16

(legend on next page)

of mechanistically driven combinations are warranted to screen for enhanced durable effects. These data further validate the identification of pathways based on isoform-switching analysis using RNA-seq datasets.

DISCUSSION

In this study, we performed isoform switch analyses using an RNA-seq dataset composed of 57 esophageal tissues across a continuum of pathologies ranging from BE with metaplasia, to BE with dysplasia (both low and high grade), and EAC. Isoform switch analyses were conducted based on histopathological progression and *TP53* mutation status given its key role in EAC progression. Our goal was to characterize isoform switching events in EAC and understand whether factors associated with increased risk for progression to EAC, namely the presence of HGD or mutant *TP53*, show unique isoform switching events that may inform future risk stratification, prevention, or therapeutic efforts.

Seventy-five genes involved in isoform switching were identified comparing low-risk with high-risk histopathologies or BE.LGD with BE.HGD groups. Inclusion of *TP53* mutation status coupled with histopathological stratification markedly increased the number of isoform-switched genes identified, resulting in 135 genes. Previously published studies suggest that alternative splicing is performed by spliceosomes and could also be controlled by RBPs, both of which are crucial components of various ribonucleoprotein (RNP) complexes.[40,41] In our data, gene-level GSEA analysis revealed many significantly enriched processes related to alternative splicing in BE.HGD compared with BE.LGD and in BE.HGD *TP53* MUT compared with BE.LGD *TP53* WT patient samples, such as ribonucleoprotein complex biogenesis, spliceosomal snRNP assembly, mRNA splice site selection, and spliceosomal complex assembly as evidenced by strong upregulation of genes in these pathways in BE.HGD compared with BE.LGD patient samples (Figure 2). For example, small nuclear ribonucleoprotein D1/2 polypeptide (*SNRPD1* and *SNRPD2*) were two of the leading-edge genes identified in both spliceosomal snRNP assembly and spliceosomal complex assembly pathways. Previously published studies suggest that overexpression of *SNRPD1* and *SNRPD2* are common in many cancers, leading to abnormal alternative splicing and regulating cell cycle and autophagy.[45,46] In EAC, *TP53* mutation is the most commonly observed mutation, with a mutation frequency over 70%.[13] *TP53* mutation is not only a driver mutation contributing to the EAC progression, but *TP53* mutations also contribute to alternative splicing activity in cancer.[47] In pancreatic ductal adenocarcinoma (PDAC), *TP53* mutations lead to significant exon usage changes and upregulate expression of RNA processing factors important for RNA splicing.[47] Therefore, aberrant RNA splicing machinery activity resulting from *TP53* mutation may explain why more isoform-switched genes are observed in the comparison of BE.LGD versus BE.HGD with the incorporation of *TP53* mutation status. Aside from significant pathway enrichment of alternative-splicing-related processes, multiple RBPs are differentially expressed on the gene level. The number of significantly altered RBPs identified are markedly increased when *TP53* mutation status is incorporated in the analysis and several RBPs have protein interactions with identified isoform-switched genes (Figures 2C and 2D). Our data support the merit of delineating specific interactions between RBPs and isoform-switched genes in future research samples using cross-linking-immunoprecipitation-sequencing. Global functional consequence analysis revealed three shared significant changes between BE.LGD versus BE.HGD and BE.LGD *TP53* WT versus BE.HGD *TP53* MUT, which are the loss of ORFs, signal peptide, and coding transcript, suggesting that dominant isoforms observed in BE.HGD, regardless of *TP53* mutation status, will have profound impact on related cellular functions, which might also be contributing factors for EAC progression.

Comprehensive analysis of isoform switching events has not previously been performed in BE or EAC. A previous pan-cancer analysis utilizing the Pan-Cancer Analysis of Whole Genomes included seven EAC cases reporting isoform-related changes in only one EAC patient when compared with non-patient-matched normal esophageal tissues from Genotype-Tissue Expression (GTEx), presenting findings as "most dominate transcripts," not isoform switching events making generalizability uncertain.[48] In addition, isoform switching of *RNF128* was previously reported in HGD and EAC.[27] *RNF128* encodes an E3 ubiquitin ligase responsible for the degradation of TP53. Similarly, we show that *RNF128* undergoes isoform switching in patients with BE.LGD compared with BE.HGD, with increased expression of *RNF128-201* and decreased expression of *RNF128-202*. *RNF128-201* has limited ubiquitin ligase activity and fails to degrade mutant TP53, whereas *RNF128-202* is the main isoform responsible for TP53 degradation.[27] Importantly, we observed a significant patient survival advantage among *RNF128-202* high expressors compared with low expressors. In addition, patients with high expression levels of *RNF128-201* had a non-significantly lower survival probability compared with patients with low expression levels (data not shown).

With the exception of *RNF128,* isoform switching events have been largely unexplored in BE and EAC. Herein, we identify large numbers of events linked to advanced pathology, as well as *TP53* mutation (as detailed in Tables S6, S7, and S8). Two reports characterizing isoform switching events in ESCC identified numerous unique isoforms with only *MINDY1* as a gene in common with our isoform switch analysis, supporting divergent molecular changes based on esophageal cancer subtype.[36,49] MINDY-1, also known as FAM63A, is a newly identified deubiquitinating protein that preferentially removes K48-linked ubiquitin molecules.[50] In BE and EAC, *MINDY1* was identified in a set of 90 genes significantly predicting disease progression by distinguishing EAC progressors from patients with non-dysplastic BE.[51]

Figure 3. GO processes associated with significant isoform switching based on histopathology and *TP53* mutation status

(A) Venn diagram showing 15 unique genes involved in isoform switching in BE.LGD versus BE.HGD, 75 unique genes involved in isoform switching in BE.LGD *TP53* WT versus BE.HGD *TP53* MUT, and 60 genes shared. (B–D) Top 10 most significant isoform-switched genes in each section of the Venn diagram ($|dIF| \geq 0.1$ and FDR ≤ 0.05). (E) GO enrichment analyses showing the top 10 enriched biological processes in each part of the Venn diagram ($p < 0.01$).

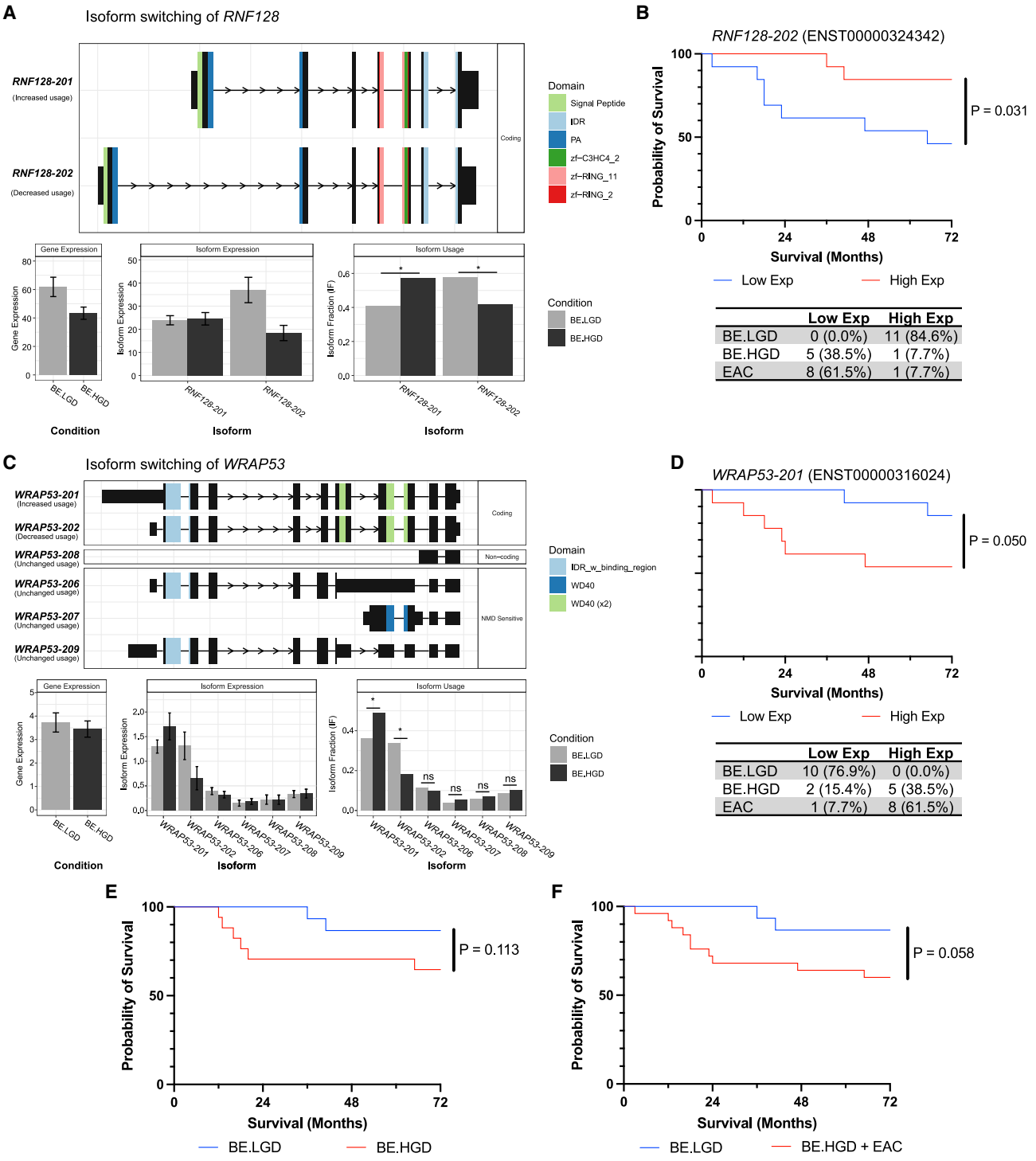

Figure 4. *TP53*-linked isoform switches predict patient survival

(A) Isoform switching of *RNF128*. Transcripts involved in isoform switching of *RNF128* and their predicted functional domain Error bars indicate 95% confidence intervals and significance levels of isoform usage were determined by the Mann–Whitney *U* test (* FDR ≤ 0.05). (B) Kaplan-Meier survival curve of patients stratified by expression level of *RNF128* transcript ENST00000324342 and the histology proportion of patients in each group. (C) Isoform switching of *WRAP53*. Transcripts of *WRAP53* and their

(legend continued on next page)

Moreover, MINDY-1 was found to promote bladder cancer progression by stabilizing YAP,[52] a key tumorigenesis pathway member that can also be induced by conjugated bile acids in EAC.[53] In our analysis, increased usage of the *MINDY1* transcript that lacks deubiquitinase (DUB) domains and a decreased usage of the *MINDY1* transcript that contains five DUB domains are observed, potentially suggesting impaired MINDY-1 function during EAC progression. Despite the fact that the *MINDY1* transcripts involved in isoform switching are different in our analysis than the data published in ESCC,[36] a similar switching trend is observed in that the isoform transcript that does not contain DUB domains is increased while the usage is decreased for a DUB domain-containing transcript. These data suggest that *MINDY1* isoforms lacking deubiquitinase domains may be important for both EAC and ESCC progression.

In ESCC, reported isoform switching events were dominated by cell regulation of cell motility, cell-to-cell junction organization, regulation of cell migration, and adhesion-linked GO processes.[49] Select isoform-switched genes in our BE progression dataset hold some similar functions. For example, isoform switching of *TPM4* was originally observed in breast cancer with loss of *TPM4.1* associated with increased migration, disruption of cell-cell adhesions, and cancer invasiveness.[32] Moreover, *TPM4.1* inhibited cellular invasion by regulating the Rac1-myosin IIB signaling.[32] Significant decreases in *TPM4.1* are observed when comparing BE.LGD with BE.HGD patients, and thus loss of *TPM4.1* during EAC progression may contribute to invasive cell behavior.[32]

Amplification and mutation of *KRAS* have been previously reported in EAC.[30,54,55] Despite the mutation frequency of *KRAS* in EAC being less than 20%, it is considered an EAC driver and proposed targeting of *KRAS* mutations may sensitize a subgroup of EAC patients to targeted treatment.[30] Alternative splicing of *KRAS* is well documented in other cancers,[33,35,56–60] resulting in two isoforms, *KRAS4A* and *KRAS4B*,[33] both of which can carry *KRAS* mutations.[33] Although expression of both *KRAS4A* and *KRAS4B* has been observed in cancer,[58] *KRAS4B* is thought to be more tumorigenic than *KRAS4A*.[33] *KRAS4A* expression inhibits apoptosis, whereas *KRAS4B* does not.[57] *KRAS4B* also regulates the matrix metalloproteinase MMP-2, which is linked to esophageal cancer development, via the PI3K-AKT signaling pathway.[56,61] Moreover, in colorectal carcinoma, expression of *KRAS4B* was found to be significantly associated with larger tumor size while expression of *KRAS4A* was significantly associated with better patient survival.[35] In our isoform switching analysis and qRT-PCR validation, we observed increased expression of *KRAS4B* and decreased expression of *KRAS4A*, suggesting that *KRAS4B* may exert a similar oncogenic role in EAC progression and warrant investigation as a therapeutic target (Figures S2C and S2D).

Interestingly, isoform switch analysis in this study also identified significant isoform-switched genes without significant differences in gene-level expression (Tables 1 and 2). Thirty-two isoform switching events (32 of 75, or 42.7%) were identified in comparing BE.LGD with BE.HGD, whereas BE.LGD *TP53* WT compared with BE.HGD *TP53* MUT resulted in identification of 62 isoform switching events (62 of 135, or 45.9%) without overall gene expression changes. GO enrichment analysis revealed similar enriched biological processes for those genes compared with enrichment analysis of all isoform-switched genes (data not shown). Isoform-switched genes that occur in the absence of altered gene-level expression include *KDM6B*, *UGT2B7*, *WRAP53*, and *TRIM29*. *KDM6B*, also known as lysine-specific demethylase 6B, is a histone demethylase that can act as either a tumor suppressor or oncogene in cancer.[62] *KDM6B* is reportedly overexpressed in pancreatic premalignancy with its expression decreasing with progression to PDAC, supporting a role for *KDM6B* in pancreatic carcinogenesis.[63] Although overall expression differences were not significant between patients with BE.LGD compared with BE.HGD, expression of the *KDM6B* coding transcript decreased while the expression of the non-coding transcript increased, suggesting *KDM6B* might also be important during early EAC progression. Conversely, *KDM6B* has been shown to promote ESCC progression and *KDM6B* levels significantly increased in patients with lymph node metastasis.[64]

As highlighted in Figure 3, the Venn diagram depicts all significant isoform-switched genes and reveals common and unique isoform switching events based on histopathology alone or both histopathology and *TP53* mutation status. Subsequent enrichment analysis revealed common and unique changes in GO biologic processes based on stratification by histopathology and *TP53* mutation status. Multiple biologic processes related to glucuronidation were among the top significantly enriched GO processes shared between two comparisons, primarily caused by significant isoform switching events observed in *UGT1A1* and *UGT2B7*. In recent years, multiple studies have shown that UDP-glucuronosyltransferase enzymes (UGTs) are linked to increased cancer risk, drug resistance, and cancer progression.[65,66] Multiple case-control studies have been published identifying associations between UGT polymorphisms and cancer risk.[65,66] It is hypothesized that UGT polymorphisms can decrease glucuronidation of carcinogens and molecules that promote cancer, such as estrogens, dietary carcinogens, and tobacco carcinogens, resulting in cancer progression.[65,67–72] However, studies have not found a significant association between UGT polymorphisms and EAC risk.[73] Based on our analysis, we identified a significant increase in the usage of a *UGT1A1* isoform that lacks a UDP-glucuronosyl and UDP-glucosyl transferase (UDPGT) domain, suggesting there is decreased glucuronidation activity of UGT1A1. Moreover, isoform switching results of *UGT2B7* showed a significant

corresponding isoform usage. Error bars indicate 95% confidence intervals and significance levels of isoform usage were determined by the Mann–Whitney *U* test, ns indicates no significant change, (* FDR $\leq$ 0.05). (D) Kaplan-Meier survival plot of patients stratified by expression of *WRAP53* transcript ENST00000316024 and histology distribution of patients in each group. (E) Survival probability of BE.LGD or BE.HGD patient samples (n = 32). (F) Patient survival probability of BE.LGD or BE.HGD + EAC (n = 41). Only the most severe pathological sample for each patient was kept in the analysis if a patient contributed multiple biopsy samples. Significance of survival differences was calculated by the Gehan-Breslow-Wilcoxon test.

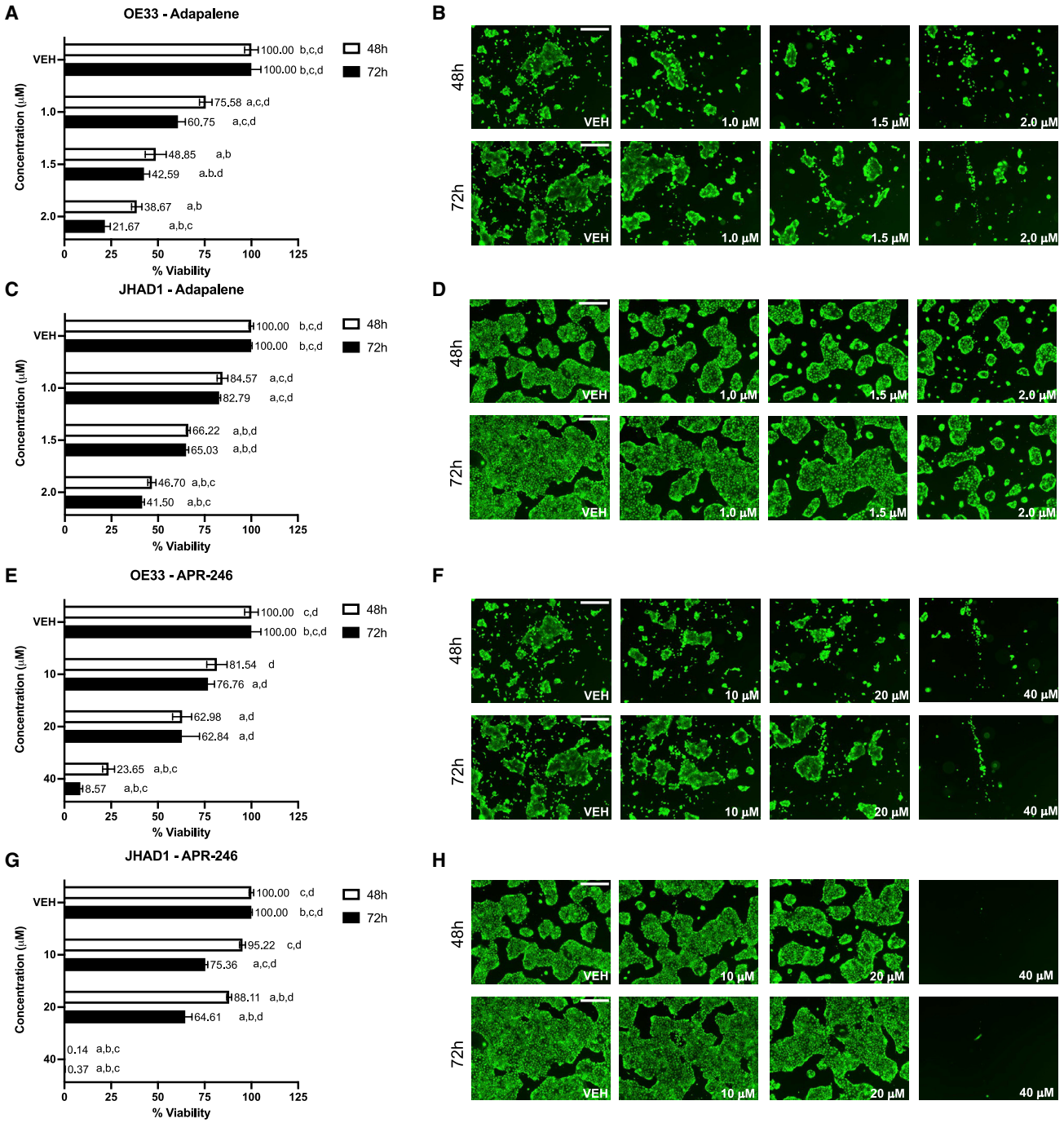

Figure 5. Enrichment analysis of isoform switching events supports retinoic acid and *TP53* signaling pathway targeting to inhibit EAC growth

(A) Viability of adapalene-treated OE33 cells measured using Calcein-AM staining 48 and 72 h post-treatment with (B) representative fluorescent images of adapalene-treated Calcein-AM stained OE33 cells. (C) Viability of adapalene-treated JHAD1 cells assessed using Calcein-AM 48 and 72 h post-treatment with (D) representative fluorescent images of adapalene-treated stained JHAD1 cells. (E) Viability of OE33 cells treated with APR-246 at 48 and 72 h post-treatment with (F) representative fluorescent images of stained OE33 cells treated with APR-246. (G) Viability of JHAD1 cells treated with APR-246 at 48 and 72 h post-treatment with (H) representative fluorescent images of stained JHAD1 cells treated with APR-246. Significant differences of viability were assessed by ANOVA with Tukey's post hoc test for multiple comparisons between treatments. Within each time point, treatments were significantly different from a = vehicle (VEH), b = 1.0 μM adapalene or 10 μM APR-246, c = 1.5 μM adapalene or 20 μM APR-246, and d = 2.0 μM adapalene or 40 μM APR-246. Data are shown as mean ± standard error. Note: VEH-48h and VEH-72h images are the same in 5B and 5F because adapalene and APR-246 treatment of OE33 cells occurred in the same plate to permit direct comparisons. Similarly, VEH-48h and VEH-72h images are the same in 5D and 5H for JHAD1 cells. Scale bars, 500 μm.

decrease in expression of the isoform that encodes a UDPGT domain, which also suggests impairment of UGT2B7 glucuronidation activity in EAC progression.

In addition, enrichment of processes related to demethylation from isoform-switched genes uniquely observed in the comparison of BE.LGD versus BE.HGD were detected. Demethylation processes in EAC have been extensively studied, and previous studies identified a key role for demethylation during disease progression, including promoter demethylation for chemokine genes and upregulation of histone demethylation proteins (KDM4C and KDM6A).[74,75] Isoform switch analysis and GO biological process enrichment analysis identified *KDM5A* and *KDM5B* as the main genes contributing to the observed enrichment of demethylation process, both of which have oncogenic roles in ESCC development but have not been assessed in EAC.[64,76] For GO processes uniquely enriched in BE.LGD *TP53* WT versus BE.HGD *TP53* MUT, processes related to retinoic acid biosynthesis and 9-*cis*-retinoic acid biosynthesis were identified (Figure 3E). Gene-level analysis revealed downregulation of associated genes with GSEA showing downregulation of retinol metabolism in patients with BE.HGD *TP53* MUT (Figure S4). Isoform switching analysis of retinol dehydrogenase 5 (*RDH5*) and aldehyde dehydrogenase 1 family member A2 (*ALDH1A2*), key proteins in the 9-*cis*-retinoic acid biosynthesis, revealed downregulation of both *RDH5* and *ALDH1A2* coding transcripts, while expression levels of non-coding transcripts were increased, further suggesting decreased activity of such processes (Table S8). Downregulation of *RDH5* has been reported in multiple types of cancer, including hepatocellular carcinoma, colon adenomas and carcinomas, and thyroid carcinoma.[77–79] In hepatocellular carcinoma, RDH5 was found to suppress proliferation and metastasis by reversing epithelial-mesenchymal transition.[79] Downregulation of *ALDH1A2* was also reported in several cancer types and suggest to act as a tumor suppressor.[80,81] Studies have also pointed out that cancer cells treated with 9-*cis*-retinoic acid induce apoptosis and inhibit cancer cell growth both *in vitro* and *in vivo*.[82,83] Moreover, retinoic acid receptor RARβ, was shown to act as a tumor suppressor in lung cancer.[84] In BE patients with LGD or HGD, expression of both *RARβ* and *RARγ* are significantly lower compared with normal esophageal tissues, and the retinoic acid-regulated nuclear protein regulation pathway is the most significantly enriched pathway in EAC progressors compared with patients with non-dysplastic BE, suggesting the potential role of retinoic acid-related processes in EAC progression.[51,85]

Significant isoform-switched genes with direct interaction with *TP53* were also identified in this study, including *RNF128*, *KDM6B*, and *WRAP53* (Figure S3). *WRAP53* has three separate alternative start exons (1α, 1β, and 1γ), which generate three different transcripts of *WRAP53* (*α*, *β*, and *γ*).[42] The precise function of *WRAP53* is largely unknown; however, it was previously reported that the 5′UTR region of *WRAP53α*, located in exon 1α, overlaps with the first exon of *TP53* and is a natural antisense of *TP53*, inducing expression of both WT and MUT *TP53*.[42] The other two forms of *WRAP53* (β and γ) do not have exon regions that overlap with exons of *TP53*.[42] In the isoform switching analysis, we observed increased expression of a *WRAP53* transcript with an overlapping exon region with *TP53* and decreased expression of a *WRAP53* transcript that does not contain an overlapping region. Moreover, protein functional domains predicted by Pfam are the same between these two isoforms. Based on this, we speculate that increased expression of a transcript with an overlapping region of *TP53* may induce expression of mutant *TP53* contributing to disease progression; however, such switching events are not likely to have a profound impact on WRAP53 function since the functional domains remain unchanged.

The Venn diagram and subsequent GO biological process analysis in Figure 3 show differences in pathway enrichment based on pathology and *TP53* mutation status, suggesting that patients stratified into different subgroups may potentially benefit from different treatment regimens. As a proof-of-principle, we used two FDA-approved drugs that target the 9-*cis*-retinoic acid pathway and *TP53* mutation to test this hypothesis. Two EAC cell lines, OE33 and JHAD1, were treated with the RARβ and RARγ agonist, adapalene, and results indicated that adapalene was a potent inducer of cell death in both cell lines. Considering RARβ and RARγ are two of the receptors of 9-*cis*-retinoic acid, these data suggest activation of 9-*cis*-retinoic acid pathway may hold potential for targeting EAC.[86] Moreover, to test the potential benefit of blocking mutant *TP53* expression in EAC, OE33 and JHAD1 cells (both *TP53* mutant) were treated with APR-246, a small molecule that restores *TP53* WT functionality.[44] Results showed that post-treatment with APR-246, both EAC cell lines experienced significant loss of viability, which is in alignment with previously published results in EAC and ESCC, although a discrepancy in effective treatment concentration of OE33 cell was noticed.[87,88] Therefore, treatment with APR-246 suggests that inhibition of mutant *TP53* expression and isoform expression linked to mutant *TP53* may be a viable preventive or treatment approach for inhibiting EAC. Moreover, enrichment of the lipid metabolism process is also observed in our analysis for BE.HGD patients that carry the *TP53* mutation. Metformin, a lipid metabolism modulating drug, was also shown to inhibit proliferation of EAC cell lines,[89] further supporting the plausibility of targeting specific pathways identified in the analysis and the importance of patient stratification based on *TP53* mutational status. Finally, epidemiological and limited preclinical data point to statins as esophageal cancer inhibitors, in alignment with agents impacting lipid metabolism holding promise in a subset of EACs.[90–94]

Treatment of EAC cells with adapalene and APR-246 shows promising results inhibiting EAC cell viability *in vitro*, suggesting that targeting specific pathways or isoforms might offer novel therapeutic insights. Genetic manipulation of specific isoforms is required to further explore the possibility of inhibiting EAC cell growth by modulating isoform expression levels. Development of synthetic splice-switching oligonucleotides may also offer a future therapeutic direction as specific isoforms are better characterized and isoform-specific inhibition showed potent results as targeted cancer therapies.[95,96] Finally, survival analysis of patients stratified by expression levels of

RNF128 and *WRAP53* isoforms showed that expression of specific isoforms could be used as prognostic markers to better predict patient survival probability. Taken together, isoform switching analysis may provide novel insights for the identification of prognostic markers and inform new potential therapeutic targets for EAC.

MATERIALS AND METHODS

RNA-seq and analysis of esophageal patient tissues

RNA was isolated from 57 esophageal tissues derived from 46 patients undergoing esophagectomy following a diagnosis of EAC or HGD at the University of Michigan as previously described.[27,97] Signed informed consent was obtained from each patient and all procedures were consistent with the protocol submitted and approved by the institutional review board. Tissue samples were collected from the tumor or within a 6 cm of the surrounding area. Histopathology of patient samples was characterized and confirmed by two independent pathologists. Patient tissues were categorized based on histopathology into the following groups: BE with metaplasia (n = 6) or LGD (n = 19) combined and referred to as BE.LGD (n = 25), BE with HGD based on >40% HGD and referred to as BE.HGD (n = 21), and EAC (n = 11) prior to RNA isolation. Total RNA was extracted using standard TRIzol methodology and all isolates had RNA integrity number greater than 7.0. Strand-specific RNA-seq library preparation and sequencing were performed at the University of Michigan Advanced Genomics Core, using the Illumina HiSeq 100-base pair paired-end sequencing platform. Quality control and adapter trimming were performed using Qiagen CLC Genomics Workbench 21.0 (https://digitalinsights.qiagen.com/). After processing, the average read count per sample was 72 million (range: 40–149 million, median: 63 million). RNA quantification and differential gene expression analysis were performed using Kallisto (version 0.46.2, 100 bootstraps with pseudoalignment saved) and Sleuth (version 0.30.0).[98,99] On average, 83% to 90% of read fragments were pseudoaligned per sample. Gencode Human Release 34 (GRCh38.p13) was used as the gene and transcript annotation source in the analysis, which contains 59,667 genes and 228,116 gene transcripts. Likelihood-ratio tests were used to determine significantly differently expressed genes by comparison groups and the Benjamini-Hochberg-adjusted FDR was applied to the analysis. Genes with p-value and FDR less than 0.05 were considered significant. Sequence files are deposited to the NCBI Gene Expression Omnibus (GEO:GSE193946) using the protocol approved by the institutional review board. *TP53* mutation analysis on patient samples was performed using the PlexSeq process by PlexSeq Diagnostics (Cleveland, OH). The lollipop plot of *TP53* mutation was generated using MutationMapper in cBioPortal.[100,101] Differentially expressed RBPs were identified using the result from Sleuth and the list of known human RBPs was acquired from a previously published study.[102]

Identification of isoform switching events

Identification of isoform switching events was performed in R (version 4.1.1) using the IsoformSwitchAnalyzeR package (version 1.14.1).[18,103] Kallisto was used to quantify transcript abundance, which was imported to the package, followed by ORF prediction and isoform switch testing using an embedded function using the DEXSeq package.[104–107] Isoform switching testing was performed by calculating the isoform fraction (IF) defined as the fraction of gene expression originating from each associated isoform, and the differential isoform fraction (dIF) value was subsequently determined by calculating the difference of IF values between two conditions of interest. Several external analyses were performed to predict functional consequences associated with isoform switching, including prediction of coding potential (CPAT),[108] coding domains (Pfam),[109] signal peptides (SignalP),[110] intrinsically disordered regions (IUPred2A),[111] and sensitivity to nonsense-mediated decay.[18,105,112,113] Results from external analyses were combined with isoform switching testing to identify isoform switch events with predicted functional consequences.[18] Results were filtered using an absolute dIF cutoff at 0.1 and FDR cutoff at 0.05. Alternative splicing analysis and genome-wide enrichment analysis were also performed.[18,103,105] Volcano plots were generated using an embedded function in the package and the dot plots were generated using ggplot2 (version 3.3.5) in R.[18,114] The Venn diagram was generated using InteractiVenn.[115] Isoform switching plots were generated directly by the IsoformSwitchAnalyzeR package. ENSEMBL transcript IDs on the isoform switching plots were matched to the corresponding transcript names. The overlapping region between *WRAP53* isoforms and *TP53* was identified using NCBI BLAST.[116]

Gene and isoform functional analysis

Comprehensive expression analysis was performed using the list of genes/transcripts that showed significant isoform switching events. The gene names of statistically significant ($|dIF| \geq 0.1$ and FDR ≤ 0.05) isoform switches for comparison groups of interest were uploaded and analyzed in Metacore and Cortellis Solution software (https://clarivate.com/products/metacore/, Clarivate Analytics, London, UK). The Enrichment Analysis, Metabolic Network, GO Molecular Function, and GO Localization tools were used to identify enriched pathways, networks, and processes that were altered in each comparison group. Significance was calculated by using the hypergeometric test and the default Metacore database with *Homo sapiens* as the background for each analysis. All p-value and FDR significant Pathway Maps, Process Networks, Diseases, GO Processes, Metabolic Networks, GO Molecular Functions, and GO Localizations for each comparison were exported for further analysis. Protein interactions between identified genes and *TP53* were predicted using the STRING database (version 11.5) with minimum required interaction score set to medium confidence (0.400) and max number of interactors to show set to query proteins only.[117] TP53 was added to the list of proteins identified from isoform-switched genes and used as input for STRING protein interaction prediction.

Gene-level GSEA

Gene-level GSEA analysis was performed as previously described.[118] In short, ranking scores of each gene were calculated using the results of differential gene expression analysis and saved as a ranked list file. The file was imported to GSEA software (version 4.2.2; Broad Institute, Cambridge, MA) and analysis was performed using GO gene sets in the Molecular Signatures Database with 1,000 permutations,

max and min size set to 500 and 15, respectively.[119–124] Leading-edge genes of each identified pathway, which were genes that contributed the most to the enrichment, were extracted from GSEA results. The heatmap and bar plots were generated using ComplexHeatmap (version 2.12.0) and ggplot2, respectively in R.[114,125] The heatmap was plotted using *z*-score-transformed transcripts per million (TPM) values of leading-edge genes.

Isoform expression determination via quantitative reverse-transcriptase PCR

cDNA for the qRT-PCR experiment was generated using the High-Capacity cDNA Reverse Transcription Kit (ThermoFisher Scientific, Waltham, MA), following the manufacturer's instructions, from RNA extracted from isolated patient samples. qRT-PCR was performed on 50 ng cDNA from BE.LGD (n = 9) and BE.HGD (n = 11) patient samples using SsoAdvanced Universal SYBR Green Supermix (Bio-Rad Laboratories, Hercules, CA) with CFX Connect Thermo Cycler (Bio-Rad Laboratories), following the manufacturer's instructions. Primer sequences for *KRAS* isoforms and *GAPDH* were acquired from previously published studies and primers for *RNF128* isoforms, *TRIM29* isoforms, and *HPRT* were designed using NCBI Primer-BLAST (Table S11).[126–128] Primers were ordered from Eurofins Scientific (Louisville, KY). Relative isoform expression was quantified against housekeeping genes (*GAPDH* and *HPRT*) and isoform fraction was calculated by dividing relative isoform expression by the total relative expression of both isoforms in a condition.

Cell culture

OE33 and JH-EsoAd1 (JHAD1) cells were cultured in RPMI 1640 medium containing 2.0 mM L-glutamine, 10^4 units/mL penicillin, 10^4 μg/mL streptomycin, 1 mM sodium pyruvate, and 10% fetal bovine serum (FBS). Cell culture reagents were acquired from either ThermoFisher Scientific or Sigma-Aldrich (St. Louis, MO). All cells were incubated at 37°C with 5% CO_2 and maintained as monolayers. The OE33 cell line was obtained from the European Collection of Authenticated Cell Cultures (ECACC, Wiltshire, UK) and the JHAD1 cell line was kindly shared by Dr. James R. Eshleman (Johns Hopkins University, Baltimore, MD).

Cellular viability assay

OE33 and JHAD1 cells were seeded in black-walled clear bottom 96-well plates at a concentration of 6,000 and 8,000 cells/well, respectively. Following overnight incubation, cells were treated with adapalene (1.0–2.0 μM; Tocris Bioscience, Bristol, UK) or APR-246 (10–40 μM; Cayman Chemical Company, Ann Arbor, MI). Treatments were prepared by diluting the stock solution to the desired experimental concentrations in RPMI 1640 medium containing 2.0 mM L-glutamine, 10^4 units/mL penicillin, 10^4 μg/mL streptomycin, 1 mM sodium pyruvate, and 5% FBS. Vehicle control was 0.08% DMSO diluted in the same medium. To determine cell viability, OE33 and JHAD1 cells were stained using Calcein-AM (ThermoFisher Scientific) at 48 and 72 h post-drug treatment as previously reported.[129] Briefly, fluorescent images and readings were acquired using the SpectraMax MiniMax Imaging Cytometer (Molecular Devices, San Jose, CA). Following the initial fluorescence reading for determining viability, cells were replenished with fresh media and incubated for another 48 h to determine whether cells recovered upon drug removal. Calcein-AM staining was similarly used to quantify recovery of viability across drug concentrations.

Statistical analysis

Survival analysis and calculation of statistical significance for viability data were performed using GraphPad Prism v9.1.0 (GraphPad Software, San Diego, CA). p-values ≤ 0.05 were considered significant unless otherwise noted. Survival analysis was performed on patients stratified by expression levels of specific transcripts. Patients were divided into tertiles based on TPM expression values for each transcript with upper compared with lower tertiles used to investigate survival differences using the Gehen-Breslow-Wilcoxon test. One-tail two-sample *t*-tests were applied to determine significant changes in isoform fraction between BE.LGD and BE.HGD patient samples in qRT-PCR experiments and statistically significant differences in cellular viability assay were determined by using a one-way ANOVA with Tukey's post hoc multiple comparisons test.

Data availability statement

RNA-sequencing files generated and analyzed during this study are available in the NCBI Gene Expression Omnibus (GEO: GSE193946).

SUPPLEMENTAL INFORMATION

Supplemental information can be found online at https://doi.org/10.1016/j.omtn.2022.08.018.

ACKNOWLEDGMENTS

We thank the National Institutes of Health and National Cancer Institute (U54CA163059) and the University of Michigan (U057239) for supporting this study. This study was additionally supported by the John and Carla Klein Family research fund awarded to L.A.K.. We also thank Dr. James R. Eshleman (Johns Hopkins University, Baltimore, MD) for sharing the JH-EsoAd1 cell line used in this study. The graphical abstract was created using BioRender (BioRender.com).

AUTHOR CONTRIBUTIONS

Conceptualization, Y.Z., K.M.W., C.L.H., and L.A.K.; methodology, Y.Z., C.L.H., J.R., J.L.C., D.G.B., and L.A.K.; software, Y.Z. C.L.H., and J.R.; validation, Y.Z., C.L.H., K.M.W., and L.A.K.; formal analysis, Y.Z. and C.L.H.; investigation, Y.Z., K.M.W., C.L.H., and L.A.K.; resources, K.H.L., J.L., R.M.R., A.C.C., D.G.B., and L.A.K.; data curation, Y.Z., K.M.W., C.L.H., J.R., D.G.B., and L.A.K.; writing—original draft preparation, Y.Z., K.M.W., C.L.H., and L.A.K.; writing—review and editing, Y.Z., K.M.W., C.L.H., J.R., J.L.C., K.H.L., J.L., R.M.R., A.C.C., D.G.B., and L.A.K.; visualization, Y.Z.; supervision, L.A.K.; project administration, L.A.K.; funding acquisition, L.A.K. All authors have read and agreed to the published version of the manuscript.

DECLARATION OF INTERESTS

The authors declare no competing interests.

REFERENCES

1. Huang, J., Koulaouzidis, A., Marlicz, W., Lok, V., Chu, C., Ngai, C.H., Zhang, L., Chen, P., Wang, S., Yuan, J., et al. (2021). Global burden, risk factors, and trends of esophageal cancer: an analysis of cancer registries from 48 countries. Cancers *13*, E141.
2. Klingelhöfer, D., Zhu, Y., Braun, M., Brüggmann, D., Schöffel, N., and Groneberg, D.A. (2019). A world map of esophagus cancer research: a critical accounting. J. Transl. Med. *17*, 150.
3. Siegel, R.L., Miller, K.D., Fuchs, H.E., and Jemal, A. (2021). Cancer statistics, 2021. CA. Cancer J. Clin. *71*, 7–33.
4. National Cancer Institute – Surveillance. Epidemiology and End Results Program (2022). Cancer Stat Facts. Esophageal Cancer. https://seer.cancer.gov/statfacts/html/esoph.html
5. Domper Arnal, M.J., Ferrández Arenas, Á., and Lanas Arbeloa, Á. (2015). Esophageal cancer: risk factors, screening and endoscopic treatment in Western and Eastern countries. World J. Gastroenterol. *21*, 7933–7943.
6. Grady, W.M., Yu, M., Markowitz, S.D., and Chak, A. (2020). Barrett's esophagus and esophageal adenocarcinoma biomarkers. Cancer Epidemiol. Biomarkers Prev. *29*, 2486–2494.
7. Kambhampati, S., Tieu, A.H., Luber, B., Wang, H., and Meltzer, S.J. (2020). Risk factors for progression of barrett's esophagus to high grade dysplasia and esophageal adenocarcinoma. Sci. Rep. *10*, 4899.
8. Stachler, M.D., Camarda, N.D., Deitrick, C., Kim, A., Agoston, A.T., Odze, R.D., Hornick, J.L., Nag, A., Thorner, A.R., Ducar, M., et al. (2018). Detection of mutations in barrett's esophagus before progression to high-grade dysplasia or adenocarcinoma. Gastroenterology *155*, 156–167.
9. Ross-Innes, C.S., Becq, J., Warren, A., Cheetham, R.K., Northen, H., O'Donovan, M., Malhotra, S., di Pietro, M., Ivakhno, S., He, M., et al. (2015). Whole-genome sequencing provides new insights into the clonal architecture of Barrett's esophagus and esophageal adenocarcinoma. Nat. Genet. *47*, 1038–1046.
10. Wani, S., Puli, S.R., Shaheen, N.J., Westhoff, B., Slehria, S., Bansal, A., Rastogi, A., Sayana, H., and Sharma, P. (2009). Esophageal adenocarcinoma in Barrett's esophagus after endoscopic ablative therapy: a meta-analysis and systematic review. Am. J. Gastroenterol. *104*, 502–513.
11. Reid, B.J., Weinstein, W.M., Lewin, K.J., Haggitt, R.C., VanDeventer, G., DenBesten, L., and Rubin, C.E. (1988). Endoscopic biopsy can detect high-grade dysplasia or early adenocarcinoma in Barrett's esophagus without grossly recognizable neoplastic lesions. Gastroenterology *94*, 81–90.
12. Nones, K., Waddell, N., Wayte, N., Patch, A.M., Bailey, P., Newell, F., Holmes, O., Fink, J.L., Quinn, M.C.J., Tang, Y.H., et al. (2014). Genomic catastrophes frequently arise in esophageal adenocarcinoma and drive tumorigenesis. Nat. Commun. *5*, 5224.
13. Dulak, A.M., Stojanov, P., Peng, S., Lawrence, M.S., Fox, C., Stewart, C., Bandla, S., Imamura, Y., Schumacher, S.E., Shefler, E., et al. (2013). Exome and whole-genome sequencing of esophageal adenocarcinoma identifies recurrent driver events and mutational complexity. Nat. Genet. *45*, 478–486.
14. Chung, S.M., Kao, J., Hyjek, E., and Chen, Y.T. (2007). p53 in esophageal adenocarcinoma: a critical reassessment of mutation frequency and identification of 72Arg as the dominant allele. Int. J. Oncol. *31*, 1351–1355.
15. Stachler, M.D., Taylor-Weiner, A., Peng, S., McKenna, A., Agoston, A.T., Odze, R.D., Davison, J.M., Nason, K.S., Loda, M., Leshchiner, I., et al. (2015). Paired exome analysis of Barrett's esophagus and adenocarcinoma. Nat. Genet. *47*, 1047–1055.
16. Killcoyne, S., and Fitzgerald, R.C. (2021). Evolution and progression of Barrett's oesophagus to oesophageal cancer. Nat. Rev. Cancer *21*, 731–741.
17. Murugaesu, N., Wilson, G.A., Birkbak, N.J., Watkins, T., McGranahan, N., Kumar, S., Abbassi-Ghadi, N., Salm, M., Mitter, R., Horswell, S., et al. (2015). Tracking the genomic evolution of esophageal adenocarcinoma through neoadjuvant chemotherapy. Cancer Discov. *5*, 821–831.
18. Vitting-Seerup, K., and Sandelin, A. (2017). The landscape of isoform switches in human cancers. Mol. Cancer Res. *15*, 1206–1220.
19. Wang, Z., Gerstein, M., and Snyder, M. (2009). RNA-Seq: a revolutionary tool for transcriptomics. Nat. Rev. Genet. *10*, 57–63.
20. Sebestyén, E., Zawisza, M., and Eyras, E. (2015). Detection of recurrent alternative splicing switches in tumor samples reveals novel signatures of cancer. Nucleic Acids Res. *43*, 1345–1356.
21. Climente-González, H., Porta-Pardo, E., Godzik, A., and Eyras, E. (2017). The functional impact of alternative splicing in cancer. Cell Rep. *20*, 2215–2226.
22. Snyder, P., Dunbar, K., Cipher, D.J., Souza, R.F., Spechler, S.J., and Konda, V.J.A. (2019). Aberrant p53 immunostaining in barrett's esophagus predicts neoplastic progression: systematic review and meta-analyses. Dig. Dis. Sci. *64*, 1089–1097.
23. Younes, M., Brown, K., Lauwers, G.Y., Ergun, G., Meriano, F., Schmulen, A.C., Barroso, A., and Ertan, A. (2017). p53 protein accumulation predicts malignant progression in Barrett's metaplasia: a prospective study of 275 patients. Histopathology *71*, 27–33.
24. Davelaar, A.L., Calpe, S., Lau, L., Timmer, M.R., Visser, M., Ten Kate, F.J., Parikh, K.B., Meijer, S.L., Bergman, J.J., Fockens, P., and Krishnadath, K.K. (2015). Aberrant TP53 detected by combining immunohistochemistry and DNA-FISH improves Barrett's esophagus progression prediction: a prospective follow-up study. Genes Chromosomes Cancer *54*, 82–90.
25. Kastelein, F., Biermann, K., Steyerberg, E.W., Verheij, J., Kalisvaart, M., Looijenga, L.H.J., Stoop, H.A., Walter, L., Kuipers, E.J., Spaander, M.C.W., et al. (2013). Aberrant p53 protein expression is associated with an increased risk of neoplastic progression in patients with Barrett's oesophagus. Gut *62*, 1676–1683.
26. Murray, L., Sedo, A., Scott, M., McManus, D., Sloan, J.M., Hardie, L.J., Forman, D., and Wild, C.P. (2006). TP53 and progression from Barrett's metaplasia to oesophageal adenocarcinoma in a UK population cohort. Gut *55*, 1390–1397.
27. Ray, D., Ray, P., Ferrer-Torres, D., Wang, Z., Nancarrow, D., Yoon, H.W., San Martinho, M., Hinton, T., Owens, S., Thomas, D., et al. (2020). Isoforms of RNF128 regulate the stability of mutant P53 in barrett's esophageal cells. Gastroenterology *158*, 583–597.e1.
28. Essakly, A., Loeser, H., Kraemer, M., Alakus, H., Chon, S.H., Zander, T., Buettner, R., Hillmer, A.M., Bruns, C.J., Schroeder, W., et al. (2020). PIK3CA and KRAS amplification in esophageal adenocarcinoma and their impact on the inflammatory tumor microenvironment and prognosis. Transl. Oncol. *13*, 157–164.
29. Jammula, S., Katz-Summercorn, A.C., Li, X., Linossi, C., Smyth, E., Killcoyne, S., Biasci, D., Subash, V.V., Abbas, S., Blasko, A., et al. (2020). Identification of subtypes of barrett's esophagus and esophageal adenocarcinoma based on DNA methylation profiles and integration of transcriptome and genome data. Gastroenterology *158*, 1682–1697.e1.
30. Frankell, A.M., Jammula, S., Li, X., Contino, G., Killcoyne, S., Abbas, S., Perner, J., Bower, L., Devonshire, G., Ococks, E., et al. (2019). The landscape of selection in 551 esophageal adenocarcinomas defines genomic biomarkers for the clinic. Nat. Genet. *51*, 506–516.
31. Miller, C.T., Moy, J.R., Lin, L., Schipper, M., Normolle, D., Brenner, D.E., Iannettoni, M.D., Orringer, M.B., and Beer, D.G. (2003). Gene amplification in esophageal adenocarcinomas and Barrett's with high-grade dysplasia. Clin. Cancer Res. *9*, 4819–4825.
32. Jeong, S., Lim, S., Schevzov, G., Gunning, P.W., and Helfman, D.M. (2017). Loss of Tpm4.1 leads to disruption of cell-cell adhesions and invasive behavior in breast epithelial cells via increased Rac1 signaling. Oncotarget *8*, 33544–33559.
33. Aran, V. (2021). K-RAS4A: lead or supporting role in cancer biology? Front. Mol. Biosci. *8*, 729830.
34. Chen, W.C., To, M.D., Westcott, P.M.K., Delrosario, R., Kim, I.J., Philips, M., Tran, Q., Bollam, S.R., Goodarzi, H., Bayani, N., et al. (2021). Targeting KRAS4A splicing through the RBM39/DCAF15 pathway inhibits cancer stem cells. Nat. Commun. *12*, 4288.
35. Abubaker, J., Bavi, P., Al-Haqawi, W., Sultana, M., Al-Harbi, S., Al-Sanea, N., Abduljabbar, A., Ashari, L.H., Alhomoud, S., Al-Dayel, F., et al. (2009). Prognostic significance of alterations in KRAS isoforms KRAS-4A/4B and KRAS mutations in colorectal carcinoma. J. Pathol. *219*, 435–445.

36. Wu, Q., Zhang, Y., An, H., Sun, W., Wang, R., Liu, M., and Zhang, K. (2021). The landscape and biological relevance of aberrant alternative splicing events in esophageal squamous cell carcinoma. Oncogene *40*, 4184–4197.

37. Paulson, T.G., Galipeau, P.C., Oman, K.M., Sanchez, C.A., Kuhner, M.K., Smith, L.P., Hadi, K., Shah, M., Arora, K., Shelton, J., et al. (2022). Somatic whole genome dynamics of precancer in Barrett's esophagus reveals features associated with disease progression. Nat. Commun. *13*, 2300.

38. Sethi, N., Kikuchi, O., McFarland, J., Zhang, Y., Chung, M., Kafker, N., Islam, M., Lampson, B., Chakraborty, A., Kaelin, W.G., Jr., and Bass, A.J. (2019). Mutant p53 induces a hypoxia transcriptional program in gastric and esophageal adenocarcinoma. JCI Insight *4*, 128439.

39. Bellini, M.F., Cadamuro, A.C.T., Succi, M., Proença, M.A., and Silva, A.E. (2012). Alterations of the TP53 gene in gastric and esophageal carcinogenesis. J. Biomed. Biotechnol. *2012*, 891961.

40. Fu, X.D., and Ares, M., Jr. (2014). Context-dependent control of alternative splicing by RNA-binding proteins. Nat. Rev. Genet. *15*, 689–701.

41. Wilkinson, M.E., Charenton, C., and Nagai, K. (2020). RNA splicing by the spliceosome. Annu. Rev. Biochem. *89*, 359–388.

42. Mahmoudi, S., Henriksson, S., Corcoran, M., Méndez-Vidal, C., Wiman, K.G., and Farnebo, M. (2009). Wrap53, a natural p53 antisense transcript required for p53 induction upon DNA damage. Mol. Cell *33*, 462–471.

43. Kim, M.J., Ciletti, N., Michel, S., Reichert, U., and Rosenfield, R.L. (2000). The role of specific retinoid receptors in sebocyte growth and differentiation in culture. J. Invest. Dermatol. *114*, 349–353.

44. Zhang, Q., Bykov, V.J.N., Wiman, K.G., and Zawacka-Pankau, J. (2018). APR-246 reactivates mutant p53 by targeting cysteines 124 and 277. Cell Death Dis. *9*, 439.

45. Dai, X., Yu, L., Chen, X., and Zhang, J. (2021). SNRPD1 confers diagnostic and therapeutic values on breast cancers through cell cycle regulation. Cancer Cell Int. *21*, 229.

46. González-Rodríguez, P., Klionsky, D.J., and Joseph, B. (2022). Autophagy regulation by RNA alternative splicing and implications in human diseases. Nat. Commun. *13*, 2735.

47. Escobar-Hoyos, L.F., Penson, A., Kannan, R., Cho, H., Pan, C.H., Singh, R.K., Apken, L.H., Hobbs, G.A., Luo, R., Lecomte, N., et al. (2020). Altered RNA splicing by mutant p53 activates oncogenic RAS signaling in pancreatic cancer. Cancer Cell *38*, 198–211.e8.

48. Kahraman, A., Karakulak, T., Szklarczyk, D., and von Mering, C. (2020). Pathogenic impact of transcript isoform switching in 1, 209 cancer samples covering 27 cancer types using an isoform-specific interaction network. Sci. Rep. *10*, 14453.

49. Ding, J., Li, C., Cheng, Y., Du, Z., Wang, Q., Tang, Z., Song, C., Xia, Q., Bai, W., Lin, L., et al. (2021). Alterations of RNA splicing patterns in esophagus squamous cell carcinoma. Cell Biosci. *11*, 36.

50. Abdul Rehman, S.A., Kristariyanto, Y.A., Choi, S.Y., Nkosi, P.J., Weidlich, S., Labib, K., Hofmann, K., and Kulathu, Y. (2016). MINDY-1 is a member of an evolutionarily conserved and structurally distinct new family of deubiquitinating enzymes. Mol. Cell *63*, 146–155.

51. Varghese, S., Newton, R., Ross-Innes, C.S., Lao-Sirieix, P., Krishnadath, K.K., O'Donovan, M., Novelli, M., Wernisch, L., Bergman, J., and Fitzgerald, R.C. (2015). Analysis of dysplasia in patients with Barrett's esophagus based on expression pattern of 90 genes. Gastroenterology *149*, 1511–1518.e5.

52. Luo, Y., Zhou, J., Tang, J., Zhou, F., He, Z., Liu, T., and Liu, T. (2021). MINDY1 promotes bladder cancer progression by stabilizing YAP. Cancer Cell Int. *21*, 395.

53. Liu, R., Li, X., Hylemon, P.B., and Zhou, H. (2018). Conjugated bile acids promote invasive growth of esophageal adenocarcinoma cells and cancer stem cell expansion via sphingosine 1-phosphate receptor 2-mediated yes-associated protein activation. Am. J. Pathol. *188*, 2042–2058.

54. Izadi, F., Sharpe, B.P., Breininger, S.P., Secrier, M., Gibson, J., Walker, R.C., Rahman, S., Devonshire, G., Lloyd, M.A., Walters, Z.S., et al. (2021). Genomic analysis of response to neoadjuvant chemotherapy in esophageal adenocarcinoma. Cancers *13*, 3394.

55. Zheng, H., Wang, Y., Tang, C., Jones, L., Ye, H., Zhang, G., Cao, W., Li, J., Liu, L., Liu, Z., et al. (2016). TP53, PIK3CA, FBXW7 and KRAS mutations in esophageal cancer identified by targeted sequencing. Cancer Genomics Proteomics *13*, 231–238.

56. Liao, J., Wolfman, J.C., and Wolfman, A. (2003). K-ras regulates the steady-state expression of matrix metalloproteinase 2 in fibroblasts. J. Biol. Chem. *278*, 31871–31878.

57. Plowman, S.J., Arends, M.J., Brownstein, D.G., Luo, F., Devenney, P.S., Rose, L., Ritchie, A.M., Berry, R.L., Harrison, D.J., Hooper, M.L., and Patek, C.E. (2006). The K-Ras 4A isoform promotes apoptosis but does not affect either lifespan or spontaneous tumor incidence in aging mice. Exp. Cell Res. *312*, 16–26.

58. Tsai, F.D., Lopes, M.S., Zhou, M., Court, H., Ponce, O., Fiordalisi, J.J., Gierut, J.J., Cox, A.D., Haigis, K.M., and Philips, M.R. (2015). K-Ras4A splice variant is widely expressed in cancer and uses a hybrid membrane-targeting motif. Proc. Natl. Acad. Sci. USA *112*, 779–784.

59. Hobbs, G.A., Der, C.J., and Rossman, K.L. (2016). RAS isoforms and mutations in cancer at a glance. J. Cell Sci. *129*, 1287–1292.

60. Nussinov, R., Tsai, C.J., Chakrabarti, M., and Jang, H. (2016). A new view of ras isoforms in cancers. Cancer Res. *76*, 18–23.

61. Palumbo, A., Jr., Meireles Da Costa, N., Pontes, B., Leite de Oliveira, F., Lohan Codeco, M., Ribeiro Pinto, L.F., and Nasciutti, L.E. (2020). Esophageal cancer development: crucial clues arising from the extracellular matrix. Cells *9*.

62. Lagunas-Rangel, F.A. (2021). KDM6B (JMJD3) and its dual role in cancer. Biochimie *184*, 63–71.

63. Yamamoto, K., Tateishi, K., Kudo, Y., Sato, T., Yamamoto, S., Miyabayashi, K., Matsusaka, K., Asaoka, Y., Ijichi, H., Hirata, Y., et al. (2014). Loss of histone demethylase KDM6B enhances aggressiveness of pancreatic cancer through downregulation of C/EBPalpha. Carcinogenesis *35*, 2404–2414.

64. Qin, M., Han, F., Wu, J., Gao, F.X., Li, Y., Yan, D.X., He, X.M., Long, Y., Tang, X.P., Ren, D.L., et al. (2021). KDM6B promotes ESCC cell proliferation and metastasis by facilitating C/EBPbeta transcription. BMC Cancer *21*, 559.

65. Hu, D.G., Mackenzie, P.I., McKinnon, R.A., and Meech, R. (2016). Genetic polymorphisms of human UDP-glucuronosyltransferase (UGT) genes and cancer risk. Drug Metab. Rev. *48*, 47–69.

66. Allain, E.P., Rouleau, M., Lévesque, E., and Guillemette, C. (2020). Emerging roles for UDP-glucuronosyltransferases in drug resistance and cancer progression. Br. J. Cancer *122*, 1277–1287.

67. Ren, Q., Murphy, S.E., Zheng, Z., and Lazarus, P. (2000). O-Glucuronidation of the lung carcinogen 4-(methylnitrosamino)-1- (3-pyridyl)-1-butanol (NNAL) by human UDP-glucuronosyltransferases 2B7 and 1A9. Drug Metab. Dispos. *28*, 1352–1360.

68. Dellinger, R.W., Chen, G., Blevins-Primeau, A.S., Krzeminski, J., Amin, S., and Lazarus, P. (2007). Glucuronidation of PhIP and N-OH-PhIP by UDP-glucuronosyltransferase 1A10. Carcinogenesis *28*, 2412–2418.

69. Itäaho, K., Mackenzie, P.I., Ikushiro, S.i., Miners, J.O., and Finel, M. (2008). The configuration of the 17-hydroxy group variably influences the glucuronidation of beta-estradiol and epiestradiol by human UDP-glucuronosyltransferases. Drug Metab. Dispos. *36*, 2307–2315.

70. Nagar, S., and Remmel, R.P. (2006). Uridine diphosphoglucuronosyltransferase pharmacogenetics and cancer. Oncogene *25*, 1659–1672.

71. Mackenzie, P.I., Miners, J.O., and McKinnon, R.A. (2000). Polymorphisms in UDP glucuronosyltransferase genes: functional consequences and clinical relevance. Clin. Chem. Lab. Med. *38*, 889–892.

72. Guillemette, C. (2003). Pharmacogenomics of human UDP-glucuronosyltransferase enzymes. Pharmacogenomics J. *3*, 136–158.

73. Dura, P., Salomon, J., Te Morsche, R.H.M., Roelofs, H.M.J., Kristinsson, J.O., Wobbes, T., Witteman, B.J.M., Tan, A.C.I.T.L., Drenth, J.P.H., and Peters, W.H.M. (2012). High enzyme activity UGT1A1 or low activity UGT1A8 and UGT2B4 genotypes increase esophageal cancer risk. Int. J. Oncol. *40*, 1789–1796.

74. Shrivastava, M.S., Hussain, Z., Giricz, O., Shenoy, N., Polineni, R., Maitra, A., and Verma, A. (2014). Targeting chemokine pathways in esophageal adenocarcinoma. Cell Cycle *13*, 3320–3327.

75. Lopes, N., Correia, M.P., Henrique, R., and Jerónimo, C. (2020). Epigenetic alterations in oesophageal cancer: expression and role of the involved enzymes. Int. J. Mol. Sci. *21*, E3522.

76. Kano, Y., Konno, M., Ohta, K., Haraguchi, N., Nishikawa, S., Kagawa, Y., Hamabe, A., Hasegawa, S., Ogawa, H., Fukusumi, T., et al. (2013). Jumonji/Arid1b (Jarid1b) protein modulates human esophageal cancer cell growth. Mol. Clin. Oncol. *1*, 753–757.

77. Lv, L., Cao, L., Hu, G., Shen, Q., and Wu, J. (2020). Methylation-driven genes identified as novel prognostic indicators for thyroid carcinoma. Front. Genet. *11*, 294.

78. Jette, C., Peterson, P.W., Sandoval, I.T., Manos, E.J., Hadley, E., Ireland, C.M., and Jones, D.A. (2004). The tumor suppressor adenomatous polyposis coli and caudal related homeodomain protein regulate expression of retinol dehydrogenase L. J. Biol. Chem. *279*, 34397–34405.

79. Hu, H., Xu, L., Luo, S.J., Xiang, T., Chen, Y., Cao, Z.R., Zhang, Y.J., Mo, Z., Wang, Y., Meng, D.F., et al. (2020). Retinal dehydrogenase 5 (RHD5) attenuates metastasis via regulating HIPPO/YAP signaling pathway in Hepatocellular Carcinoma. Int. J. Med. Sci. *17*, 1897–1908.

80. Chang, P.M.H., Chen, C.H., Yeh, C.C., Lu, H.J., Liu, T.T., Chen, M.H., Liu, C.Y., Wu, A.T.H., Yang, M.H., Tai, S.K., et al. (2018). Transcriptome analysis and prognosis of ALDH isoforms in human cancer. Sci. Rep. *8*, 2713.

81. Choi, J.A., Kwon, H., Cho, H., Chung, J.Y., Hewitt, S.M., and Kim, J.H. (2019). ALDH1A2 is a candidate tumor suppressor gene in ovarian cancer. Cancers *11*.

82. Eskra, J.N., Kuiper, J.W., Walden, P.D., Bosland, M.C., and Özten, N. (2017). Interactive effects of 9-cis-retinoic acid and androgen on proliferation, differentiation, and apoptosis of LNCaP prostate cancer cells. Eur. J. Cancer Prev. *26*, 71–77.

83. Naka, K., Yokozaki, H., Domen, T., Hayashi, K., Kuniyasu, H., Yasui, W., Lotan, R., and Tahara, E. (1997). Growth inhibition of cultured human gastric cancer cells by 9-cis-retinoic acid with induction of cdk inhibitor Waf1/Cip1/Sdi1/p21 protein. Differentiation. *61*, 313–320.

84. Houle, B., Rochette-Egly, C., and Bradley, W.E. (1993). Tumor-suppressive effect of the retinoic acid receptor beta in human epidermoid lung cancer cells. Proc. Natl. Acad. Sci. USA *90*, 985–989.

85. Lord, R.V., Tsai, P.I., Danenberg, K.D., Peters, J.H., Demeester, T.R., Tsao-Wei, D.D., Groshen, S., Salonga, D., Park, J.M., Crookes, P.F., et al. (2001). Retinoic acid receptor-alpha messenger RNA expression is increased and retinoic acid receptor-gamma expression is decreased in Barrett's intestinal metaplasia, dysplasia, adenocarcinoma sequence. Surgery *129*, 267–276.

86. Rusu, A., Tanase, C., Pascu, G.A., and Todoran, N. (2020). Recent advances regarding the therapeutic potential of adapalene. Pharmaceuticals *13*, E217.

87. Liu, D.S.H., Read, M., Cullinane, C., Azar, W.J., Fennell, C.M., Montgomery, K.G., Haupt, S., Haupt, Y., Wiman, K.G., Duong, C.P., et al. (2015). APR-246 potently inhibits tumour growth and overcomes chemoresistance in preclinical models of oesophageal adenocarcinoma. Gut *64*, 1506–1516.

88. Kobayashi, T., Makino, T., Yamashita, K., Saito, T., Tanaka, K., Takahashi, T., Kurokawa, Y., Yamasaki, M., Nakajima, K., Morii, E., et al. (2021). APR-246 induces apoptosis and enhances chemo-sensitivity via activation of ROS and TAp73-Noxa signal in oesophageal squamous cell cancer with TP53 missense mutation. Br. J. Cancer *125*, 1523–1532.

89. Fujihara, S., Kato, K., Morishita, A., Iwama, H., Nishioka, T., Chiyo, T., Nishiyama, N., Miyoshi, H., Kobayashi, M., Kobara, H., et al. (2015). Antidiabetic drug metformin inhibits esophageal adenocarcinoma cell proliferation in vitro and in vivo. Int. J. Oncol. *46*, 2172–2180.

90. Alexandre, L., Clark, A.B., Bhutta, H.Y., Holt, S., Lewis, M.P.N., and Hart, A.R. (2014). Statin use is associated with reduced risk of histologic subtypes of esophageal cancer: a nested case-control analysis. Gastroenterology *146*, 661–668.

91. Nguyen, T., Duan, Z., Naik, A.D., Kramer, J.R., and El-Serag, H.B. (2015). Statin use reduces risk of esophageal adenocarcinoma in US veterans with Barrett's esophagus: a nested case-control study. Gastroenterology *149*, 1392–1398.

92. Ogunwobi, O.O., and Beales, I.L.P. (2008). Statins inhibit proliferation and induce apoptosis in Barrett's esophageal adenocarcinoma cells. Am. J. Gastroenterol. *103*, 825–837.

93. Nguyen, D.M., Richardson, P., and El-Serag, H.B. (2010). Medications (NSAIDs, statins, proton pump inhibitors) and the risk of esophageal adenocarcinoma in patients with Barrett's esophagus. Gastroenterology *138*, 2260–2266.

94. Singh, S., Singh, A.G., Singh, P.P., Murad, M.H., and Iyer, P.G. (2013). Statins are associated with reduced risk of esophageal cancer, particularly in patients with Barrett's esophagus: a systematic review and meta-analysis. Clin. Gastroenterol. Hepatol. *11*, 620–629.

95. Li, F.Y., Zhang, Z.F., Voss, S., Wu, Y.W., Zhao, Y.F., Li, Y.M., and Chen, Y.X. (2019). Inhibition of K-Ras4B-plasma membrane association with a membrane microdomain-targeting peptide. Chem. Sci. *11*, 826–832.

96. Wang, X., Ding, J., and Meng, L.H. (2015). PI3K isoform-selective inhibitors: next-generation targeted cancer therapies. Acta Pharmacol. Sin. *36*, 1170–1176.

97. Lagisetty, K.H., McEwen, D.P., Nancarrow, D.J., Schiebel, J.G., Ferrer-Torres, D., Ray, D., Frankel, T.L., Lin, J., Chang, A.C., Kresty, L.A., and Beer, D.G. (2021). Immune determinants of Barrett's progression to esophageal adenocarcinoma. JCI Insight *6*, 143888.

98. Bray, N.L., Pimentel, H., Melsted, P., and Pachter, L. (2016). Near-optimal probabilistic RNA-seq quantification. Nat. Biotechnol. *34*, 525–527.

99. Pimentel, H., Bray, N.L., Puente, S., Melsted, P., and Pachter, L. (2017). Differential analysis of RNA-seq incorporating quantification uncertainty. Nat. Methods *14*, 687–690.

100. Cerami, E., Gao, J., Dogrusoz, U., Gross, B.E., Sumer, S.O., Aksoy, B.A., Jacobsen, A., Byrne, C.J., Heuer, M.L., Larsson, E., et al. (2012). The cBio cancer genomics portal: an open platform for exploring multidimensional cancer genomics data. Cancer Discov. *2*, 401–404.

101. Gao, J., Aksoy, B.A., Dogrusoz, U., Dresdner, G., Gross, B., Sumer, S.O., Sun, Y., Jacobsen, A., Sinha, R., Larsson, E., et al. (2013). Integrative analysis of complex cancer genomics and clinical profiles using the cBioPortal. Sci. Signal. *6*, pl1.

102. Hu, G., Jiang, Q., Liu, L., Peng, H., Wang, Y., Li, S., Tang, Y., Yu, J., Yang, J., and Liu, Z. (2020). Integrated analysis of RNA-binding proteins associated with the prognosis and immunosuppression in squamous cell carcinoma of head and neck. Front. Genet. *11*, 571403.

103. Vitting-Seerup, K., and Sandelin, A. (2019). IsoformSwitchAnalyzeR: analysis of changes in genome-wide patterns of alternative splicing and its functional consequences. Bioinformatics *35*, 4469–4471.

104. Soneson, C., Love, M.I., and Robinson, M.D. (2015). Differential analyses for RNA-seq: transcript-level estimates improve gene-level inferences. F1000Res. *4*, 1521.

105. Vitting-Seerup, K., Porse, B.T., Sandelin, A., and Waage, J. (2014). spliceR: an R package for classification of alternative splicing and prediction of coding potential from RNA-seq data. BMC Bioinf. *15*, 81.

106. Anders, S., Reyes, A., and Huber, W. (2012). Detecting differential usage of exons from RNA-seq data. Genome Res. *22*, 2008–2017.

107. Ritchie, M.E., Phipson, B., Wu, D., Hu, Y., Law, C.W., Shi, W., and Smyth, G.K. (2015). Limma powers differential expression analyses for RNA-sequencing and microarray studies. Nucleic Acids Res. *43*, e47.

108. Wang, L., Park, H.J., Dasari, S., Wang, S., Kocher, J.P., and Li, W. (2013). CPAT: coding-Potential Assessment Tool using an alignment-free logistic regression model. Nucleic Acids Res. *41*, e74.

109. Punta, M., Coggill, P.C., Eberhardt, R.Y., Mistry, J., Tate, J., Boursnell, C., Pang, N., Forslund, K., Ceric, G., Clements, J., et al. (2012). The Pfam protein families database. Nucleic Acids Res. *40*, D290–D301.

110. Almagro Armenteros, J.J., Tsirigos, K.D., Sønderby, C.K., Petersen, T.N., Winther, O., Brunak, S., von Heijne, G., and Nielsen, H. (2019). SignalP 5.0 improves signal peptide predictions using deep neural networks. Nat. Biotechnol. *37*, 420–423.

111. Mészáros, B., Erdős, G., and Dosztányi, Z. (2018). IUPred2A: context-dependent prediction of protein disorder as a function of redox state and protein binding. Nucleic Acids Res. *46*, W329–W337.

112. Weischenfeldt, J., Waage, J., Tian, G., Zhao, J., Damgaard, I., Jakobsen, J.S., Kristiansen, K., Krogh, A., Wang, J., and Porse, B.T. (2012). Mammalian tissues defective in nonsense-mediated mRNA decay display highly aberrant splicing patterns. Genome Biol. *13*, R35.

113. Huber, W., Carey, V.J., Gentleman, R., Anders, S., Carlson, M., Carvalho, B.S., Bravo, H.C., Davis, S., Gatto, L., Girke, T., et al. (2015). Orchestrating high-throughput genomic analysis with Bioconductor. Nat. Methods *12*, 115–121.

114. Wickham, H. (2016). ggplot2: Elegant Graphics for Data Analysis (New York: Springer-Verlag).

115. Heberle, H., Meirelles, G.V., da Silva, F.R., Telles, G.P., and Minghim, R. (2015). InteractiVenn: a web-based tool for the analysis of sets through Venn diagrams. BMC Bioinf. *16*, 169.

116. Zhang, Z., Schwartz, S., Wagner, L., and Miller, W. (2000). A greedy algorithm for aligning DNA sequences. J. Comput. Biol. *7*, 203–214.

117. Szklarczyk, D., Franceschini, A., Wyder, S., Forslund, K., Heller, D., Huerta-Cepas, J., Simonovic, M., Roth, A., Santos, A., Tsafou, K.P., et al. (2015). STRING v10: protein-protein interaction networks, integrated over the tree of life. Nucleic Acids Res. *43*, D447–D452.

118. Reimand, J., Isserlin, R., Voisin, V., Kucera, M., Tannus-Lopes, C., Rostamianfar, A., Wadi, L., Meyer, M., Wong, J., Xu, C., et al. (2019). Pathway enrichment analysis and visualization of omics data using g:Profiler, GSEA, Cytoscape and EnrichmentMap. Nat. Protoc. *14*, 482–517.

119. Gene Ontology Consortium (2021). The Gene Ontology resource: enriching a GOld mine. Nucleic Acids Res. *49*, D325–D334.

120. Liberzon, A., Subramanian, A., Pinchback, R., Thorvaldsdóttir, H., Tamayo, P., and Mesirov, J.P. (2011). Molecular signatures database (MSigDB) 3.0. Bioinformatics *27*, 1739–1740.

121. Liberzon, A., Birger, C., Thorvaldsdóttir, H., Ghandi, M., Mesirov, J.P., and Tamayo, P. (2015). The Molecular Signatures Database (MSigDB) hallmark gene set collection. Cell Syst. *1*, 417–425.

122. Ashburner, M., Ball, C.A., Blake, J.A., Botstein, D., Butler, H., Cherry, J.M., Davis, A.P., Dolinski, K., Dwight, S.S., Eppig, J.T., et al. (2000). Gene ontology: tool for the unification of biology. The Gene Ontology Consortium. Nat. Genet. *25*, 25–29.

123. Subramanian, A., Tamayo, P., Mootha, V.K., Mukherjee, S., Ebert, B.L., Gillette, M.A., Paulovich, A., Pomeroy, S.L., Golub, T.R., Lander, E.S., and Mesirov, J.P. (2005). Gene set enrichment analysis: a knowledge-based approach for interpreting genome-wide expression profiles. Proc. Natl. Acad. Sci. USA *102*, 15545–15550.

124. Mootha, V.K., Lindgren, C.M., Eriksson, K.F., Subramanian, A., Sihag, S., Lehar, J., Puigserver, P., Carlsson, E., Ridderstråle, M., Laurila, E., et al. (2003). PGC-1alpha-responsive genes involved in oxidative phosphorylation are coordinately downregulated in human diabetes. Nat. Genet. *34*, 267–273.

125. Gu, Z., Eils, R., and Schlesner, M. (2016). Complex heatmaps reveal patterns and correlations in multidimensional genomic data. Bioinformatics *32*, 2847–2849.

126. Dahn, M.L., Dean, C.A., Jo, D.B., Coyle, K.M., and Marcato, P. (2021). Human-specific GAPDH qRT-PCR is an accurate and sensitive method of xenograft metastasis quantification. Mol. Ther. Methods Clin. Dev. *20*, 398–408.

127. Newlaczyl, A.U., Coulson, J.M., and Prior, I.A. (2017). Quantification of spatiotemporal patterns of Ras isoform expression during development. Sci. Rep. *7*, 41297.

128. Ye, J., Coulouris, G., Zaretskaya, I., Cutcutache, I., Rozen, S., and Madden, T.L. (2012). Primer-BLAST: a tool to design target-specific primers for polymerase chain reaction. BMC Bioinf. *13*, 134.

129. Weh, K.M., Howell, A.B., and Kresty, L.A. (2016). Expression, modulation, and clinical correlates of the autophagy protein Beclin-1 in esophageal adenocarcinoma. Mol. Carcinog. *55*, 1876–1885.